



Sensitivity of the blocking-North Atlantic Oscillation relationship to index

Kayla Besong¹ · Ben Kirtman¹

Received: 21 April 2022 / Accepted: 16 September 2023 / Published online: 4 October 2023
© The Author(s), under exclusive licence to Springer-Verlag GmbH Germany, part of Springer Nature 2023

Abstract

North Atlantic blocking and the North Atlantic Oscillation (NAO) are two phenomena that have been extensively studied due to their significant spatio-temporal overlap. This work presents an index comparison study applied to this relationship, bringing light to how the strength of it varies considerably depending on blocking index choice and why this could be leading to discrepancies found in previous works. A PV– θ blocking index is used alongside a direction of breaking metric to classify blocking as either cyclonic or anticyclonic based on the Rossby wave breaking occurring at onset. These results are compared against those found using an absolute geopotential height (AGP) index. The analysis is performed using both area-averaged blocking count during winter and at each grid-point across the North Atlantic for all seasons. The study demonstrates that the choice of method significantly affects the results when correlating wintertime blocking and NAO. Blocks found using the AGP index show a much stronger correlation with the NAO compared to those found with the PV– θ index. Other analyses, such as frequency, duration, and composites, suggest that the AGP algorithm detects stronger, more mature, and persistent blocks, which promote a higher correlation with the NAO compared to the shorter-lived PV– θ blocks. Based on this analysis, it can be concluded that different blocking events are being measured between the two indices, contributing to the stark differences in the correlation analysis, each with their own advantages and disadvantages in relating blocking to the NAO.

Keywords Blocking · NAO · Subseasonal · Rossby wave

1 Introduction

Atmospheric blocking is a quasi-stationary weather pattern best known to divert or split zonal flow in the mid to high latitudes at subseasonal time scales (Elliott and Smith 1949; Rex 1950). Blocks are characterized by anomalous anticyclones with trapped cyclones along their southern edge, representing a large-scale reversal of the meridional gradient. Minimum duration of blocking events is five days (Masato et al. 2009) which, paired with their stationarity, leads to extended influence on weather both locally as well as up-and-downstream of their centers. Local alteration of the radiation budget and temperature advection from the anomalous blocking anticyclone are directly linked to extreme temperatures (Trigo et al. 2004; Pfahl and Wernli

2012; Takaya and Nakamura 2005), heat waves (Demirtaş 2018) and wildfires (Bondur et al. 2020). Diversion of the jet stream and storm track also link blocking to extreme precipitation events, such as atmospheric rivers (Benedict et al. 2019) and drought (Wise 2016).

Extremes in local weather are accompanied by large impacts on human and natural systems, providing continuous motivation to study blocking. Further motivation stems from the fact that we do not fully comprehend the blocking lifecycle from a dynamical perspective (Woollings et al. 2018). Lack of theoretical agreement on blocking is due to their equivalent barotropic structure (Rex 1950), nonlinear interaction with planetary and synoptic scale flows (Legras and Ghil 1985; Lejenäs and Madden 1992; Ma and Lang 2017), and small to synoptic scale eddy forcing (Charney and Devore 1979; Nakamura 1994; Colucci 2001).

While planetary scale interactions and eddy forcing theories are favorably recognized here, other notable blocking theories include the modon, soliton solution (McWilliams 1980; Haines and Marshall 1987), tropical forcing (Hoskins and Karoly 1981) explosive cyclogenesis (Colucci 1985)

✉ Kayla Besong
kayla.besong@rsmas.miami.edu

¹ Department of Atmospheric Science, University of Miami
Rosenstiel School of Marine and Atmospheric Science,
Miami, FL, USA

and recently, unstable periodic orbits (Lucarini and Gritsun 2019). While all these theories describe blocked atmospheric flow and provide insight to blocking mechanisms, the problem is largely non-linear and remains a challenge.

This is reflected in our ability to capture and predict blocking in both weather forecast and climate models (Tibaldi et al. 1994; D'Andrea et al. 1998; Davini and Cagnazzo 2013). Particularly true over Greenland and the Euro-Atlantic regions, models consistently underestimate the winter blocking frequency (D'Andrea et al. 1998; Scaife et al. 2010). Ways to better predict blocking in climate models have included increasing horizontal resolution (Davini et al. 2017; Jung et al. 2012), improving model mean state bias (Scaife et al. 2010), and using fully coupled ocean-atmosphere models to better resolve sea surface temperatures (SST; Scaife et al. 2011). While all methods have yielded results that are model dependent, some improvements in overall blocking frequency bias have been shown in CMIP6 model outputs, though only on the order of ~2 to 3% (Davini and D'Andrea 2020).

As with most climate related phenomenon, to improve predictability and better understand blocking, teleconnections have been often leveraged. Of the most related to blocking are the Pacific North American (PNA) and North Atlantic Oscillation (NAO) (Crocì-Maspoli et al. 2007; Fei et al. 2002). The relationship of the NAO and blocking in the North Atlantic has been heavily studied as the NAO essentially is a measure of wind variability (Woollings et al. 2008) in the region and blocking, occurring frequently there, contributes to that variability. The NAO also represents meridional dipoles of geopotential height with the negative phase representing a reversal of that gradient, a pattern identical to Rex or dipole blocking. Are they then the same phenomenon? If so, surely if we predict one, we should be able to predict the other? This notion was applied in Athanasiadis et al. (2020) looking at decadal predictability of North Atlantic climate variability through the lens of the Atlantic Multi-decadal Variability (AMV), finding strong anticorrelations between the NAO and high latitude blocking (HLB) over Greenland (-0.95) at extended, smoothed timescales in the process. Woollings et al. (2008; hereafter W08) presented a strong case for HLB and the NAO- being the same phenomenon revealing seasonal correlation values of -0.84 unsmoothed, -0.93 smoothed and an instantaneous lag lead correlation of -0.55 . W08 ultimately concluded that the North Atlantic has only two states, blocked (NAO-) and unblocked (NAO+).

Conversely a theory from Shabbar et al. (2001) showed that the NAO and blocking are related through differential surface heating between the ocean and land, proposed using a simplified low-order theoretical model by Charney and Devore (1979) to provide dynamical explanation for the statistical relationship between the NAO and blocking

initially found. Further, Crocì-Maspoli et al. (2007) suggest that blocking and the NAO share temporal co-variability in which NAO phases can precondition blocking, help sustain their duration depending on location, and even that blocks can instigate NAO phase transitions. Similarly to Crocì-Maspoli et al. (2007), Yao and Luo (2018) who, when considering instantaneous blocking, argued that the blocking-NAO relationship as an asymmetric spatiotemporal connection with resulting asymmetric impacts on Europe.

The exact relationship of the NAO and blocking in the North Atlantic is unclear, falling into the category of the same, not the same, and/or sometimes the same phenomenon—likely attributable to spatiotemporal overlap, inferred from a combination of theories presented above and favoring that of Yao and Luo (2018). What is clear is that this relationship can be leveraged to improve understanding and predictive skill of blocking at a range of timescales. As in Athanasiadis et al. (2020) who showed slight differences in predictability of blocking and NAO when applying linear detrending at decadal timescales and in Ferranti et al. (2018) who used NAO-blocking phase transitions to show blocking itself and NAO+ are the best predictors of Scandinavian blocking at subseasonal timescales.

However, the spatio-temporal variability of the NAO-blocking relationship challenges this leverage in that the result is dependent on the analysis technique used. Supporting this argument are results Scherrer et al. (2006) who found a negative blocking/NAO correlation west, positive blocking/NAO correlation east—a result similar to Yao and Luo (2018)—found a high sensitivity of that correlation to latitude-longitude and to varying indices. Further support of sensitivity to index is derived from Pinheiro et al. (2019) who, in their comprehensive two-dimensional blocking index comparison study, cautioned that correlating blocking events spatially to other phenomenon such as extreme weather will lead to different results depending on the index used. In addition to index, sensitivity to not only region, but also sub-region in blocking analysis has revealed differences in blocking dynamics. This was displayed in Davini et al. (2017) who showed blocks over the Greenland region tended to have a baroclinic tilt compared to those over the European region having barotropic structure.

Further, a paper by Sousa et al. (2021) discusses how the lack of consistency in blocking analysis inhibits our ability to make generalized statements about blocking. They provide an in-depth review and conceptual model of blocking phenomenology in a strong effort to reduce the myriad blocking methodology and establish a consistency that is called for. The model provides distinction for omega and Rex blocking structures as well as subtropical ridges, allowing for a more comprehensive understanding of the blocking lifecycle, structures, and associated impacts. The lack in ability of the indices to distinguish and capture different

blocking structures that are applied here becomes a focal point in potentially why different results in the blocking–NAO relationship between the indices emerge.

The primary goal of this study is to show how choice of blocking index leads to varying strengths of the blocking–NAO relationship that could be contributing to discrepancies of it found throughout the literature. The methodological approach is described in section two where a PV– θ index, adopted from Masato et al. (2011, 2013; hereafter M13), is combined with classification of blocking events based on the Rossby wave breaking type driving onset. A complete climatology of cyclonic and anticyclonic blocks is provided, the frequency in Sect. 3.1 and composites in the Appendix. Correlation of blocking count with the NAO are provided in Sect. 3.2 and duration analysis in Sect. 3.3.

2 Methods

The European Center for Medium-Range Weather Forecasts (ECMWF) ERA-5 reanalysis dataset (Hersbach et al. 2020) at $0.25^\circ \times 0.25^\circ$ horizontal resolution was obtained from December 1979 to November 2019 for a 40-year study. Six-hourly outputs were averaged into daily values for all variables except for the precipitation which was obtained from the CPC Global Unified Precipitation dataset provided by the NOAA/OAR/ESRL PSL, Boulder, Colorado, USA, from their Web site at <https://psl.noaa.gov/data/gridded/data.cpc.globalprecip.html>. Potential temperature (θ) was computed on a PV = 2 potential vorticity units (PVU; $1 \text{ PVU} = 10^{-6} \text{ km}^2 \text{ kg}^{-1} \text{ s}^{-1}$) surface. Seasonal data evaluation follows December–February (DJF), March–May (MAM), June–August (JJA), and September–November (SON). All significance testing was done using a student’s *t*-test at the 95th percentile.

2.1 Blocking indices and classification

2.1.1 The PV– θ index

Methods from Masato et al. (2013; hereafter M13) were largely followed in this study with some deviation in temporal constraint and blocking classification. M13 utilized a two-dimensional adaptation of the original Pelly and Hoskins (2003) PV– θ index, following Berrisford et al. (2007) and W08. This index considers when a meridional reversal of the PV gradient occurs and can be considered as a metric to measure Rossby wave breaking (Pelly and Hoskins 2003). The 2-D instantaneous wave breaking index, *B*, is measured at each latitude (ϕ), longitude (*i*) point within the range of 75°N – 40°N with $\Delta\phi = 30^\circ$. Positive values of *B*, the difference between northern ($\bar{\theta}_i^n$) and southern ($\bar{\theta}_i^s$)

integrated theta, indicate a wave breaking event and potential for the onset of blocking.

Wave breaking alone does not equate to a blocking event but does provide the means for blocking to occur if the low-PV air from the wave break becomes fully cut-off and supported by the background flow to form an anticyclonic circulation that is both quasi-stationary and persistent (Hoskins et al. 1985). With that, the spatial constraint of the 2-D PV– θ index in this study follows the tracking algorithm in M13 where exact details can be found. The methods of M13, discussed below, were slightly more complex in applying temporal constraint. Here, to be considered a blocking event, the M13 tracking algorithm must be met for a minimum of 5 days.

When computing the blocking frequency based on $B > 0$ for blocking events, positive *B* only in the region constrained by the latitude–longitude box from step 4 of the tracking algorithm in M13 is considered, per centroid, per day. If all $B > 0$ outside of the blocking region are included in the frequency calculation for a blocking event day, blocking frequency values are much higher, approaching 50% in regions, and resemble that of M13 and W08. By limiting the frequency to spatial area of the blocking event, frequency values are similar to other blocking indices such as those seen in Davini et al. (2012) and sector blocking in Tyrllis and Hoskins (2008a).

2.1.2 K-means testing and classification

In Masato et al. (2011), two one-dimensional classification metrics—complimentary to the PV– θ index—were developed to determine the direction of breaking (DB) and relative intensity (RI) of the air mass associated with the wave breaking event. The DB takes the difference in longitude values of averaged $\bar{\theta}_i^n$ and $\bar{\theta}_i^s$. Positive DB values indicate anticyclonic and negative, cyclonic. RI is the difference in averaged $\bar{\theta}_i^n$ and $\bar{\theta}_i^s$ and 40+ year seasonal theta climatology for that given longitude point ($\bar{\theta}_i^s$). Positive RI values indicate ‘warm’ and negative, ‘cold’. From this, a phase-space plot (c.f. Fig. 3 in M11) based on DB and RI values with DB along the x-axis and RI the y-axis is developed and depending on where a given centroid lies in the phase space, determines its classification. For example, negative values of both metrics would indicate ‘cold’-cyclonic and positive values of both, ‘warm’-anticyclonic.

The DB-RI phase space in M13—who, similarly to the PV– θ index, extended the M11 metrics to 2-D form—provides a framework to apply k-means clustering to wave breaking events who met the spatial constraints set by the tracking algorithm. K-means also allows for classification and temporal constraint to be combined into one analysis technique where resulting vectors from the applied

k-means Euclidean distance calculation are a function of DB and RI with length $I = 5days$.

K-means clustering was attempted but ultimately not used in this study. Temporal constraint and classification based on the DB index only were performed manually. The reason for excluding the RI metric was in result of exhaustive clustering tests using $k=2, 3$, and 4 globally and regionally. While the results led to similar blocking frequency signatures and were robust regardless of the number of k-means trials, the blocking clusters on the phase space plot and physical interpretation of these clusters differed from M13. The primary reason for this difference was that the distribution of DB and RI values did not have large enough spread or discreteness in comparison, they were, for the most part, normally distributed about the x- and y-axes. The values were standardized by dividing by the standard deviation, as in M13 though the analysis was also tested without doing so. The results of no standardization led to the same x- and y-axis spread, but the values were skewed or shifted below the y-axis so that regardless of the direction of the wave breaking signature, the relative intensity of the air masses were largely considered 'cold'. These results suggested a possible warming signal in the potential temperature climatology, especially with this 40-year study being shifted 20 years later than that of M13. When the climatological values used to compute RI were linearly detrended, the results of the clustering resembled the original standardized results, no longer skewed but still with little spread.

The importance of the lack of spread is that when $k > 2$, the third and or fourth clusters become a mixed classification straddling the y-axis that is either 'cold'-cyclonic or 'cold'-anticyclonic depending on where you are in the cluster. Individual events were evaluated in these classifications but presented a lack of clear and distinct physical interpretation. The individual event analysis of these mixed clusters implies that k-means clustering beyond $k=2$ may not be an appropriate method for blocking classification in this study. The lack of spread in the RI values and mixed interpretation, are the reasons why the RI index was not used for classification of blocking here.

The DB index, however, is still very useful in classifying types of blocking events even if the clustering framework is not. Therefore, manual classification of DB for each day of each blocking event was ultimately evaluated. This not only allows for a clearer representation of what type of wave breaking is occurring during onset, but also blocked days in an event beyond day 5 is easily classified, giving way to more information on the day-to-day evolution of the blocking event. Classification of a blocking event as either cyclonic or anticyclonic depends on the DB value of day 0. Sensitivity tests to classification of the event based on the average DB value throughout duration or ranges varying in

the first -2 to 3 days of the event did not significantly alter blocking frequency results (not shown).

2.1.3 AGP index

Lastly, a secondary index derived in Davini et al. (2012) using geopotential height has been used throughout the study to compare with results from the PV- θ index. This index will be referenced throughout this paper as the absolute geopotential height AGP index. The methodology considers the reversal of the Z500mb gradient at each grid point in 35–75°N. A large-scale block (LSB) is an instantaneous block (IB) that persists for at least 15° longitude centered at the given latitude, longitude point. A blocking event is ultimately declared when these criteria have persisted within a 5° latitude \times 10° longitude box centered around that point for a minimum of 5 days.

2.2 Distinction in blocking type

In Sousa et al. (2021) they distinguish between different types of blocking structures such as subtropical ridges, Rex (dipole) blocks, and Omega blocks. Subtropical ridges, in an older sense were constituted as low latitude blocks (Davini et al. 2012). However, Sousa et al. shows that subtropical ridges do have importance and influence, along with omega structures that develop in the mid-to-low latitudes. Rex blocking, mature dipole blocks, or 'canonical' blocking is typically found slightly higher in latitude and 'polar blocks' or those occurring above 75°N (Sousa et al. 2021). Older denotations of high latitude blocking (HLB) are typically blocks that occur on the poleward side of the jet. This can be taken a step further where blocking over Greenland, HLB, the negative NAO, and cyclonically driven blocks are all the same things as in Woollings et al. (2008). In this study, blocks produced by the PV- θ and AGP indices are not low-latitude or polar blocks but fall more into 'canonical' and dissecting the difference between HLB, NAO-, and cyclonic blocking over Greenland becomes a point of interest.

Lastly, it is noted here that other indices may use a shorter or longer temporal criteria, though for consistency with the lineage of indices used here, we continue with a 5-day minimum.

3 Results

The primary goal of this study is to show how choice of blocking index leads to varying strengths of the blocking-NAO relationship. Although extensive work exists on blocking climatology, supplemental analysis from the PV- θ index with DB classification are provided for context, comparison with other studies, and future reference. The first section

highlights an updated, two-dimensional, seasonally averaged, classified climatological blocking frequency computed over 40-years from the PV- θ index. Composite anomalies of various weather-related variables such as sea surface temperatures and precipitation during blocking events are presented alongside NAO composites in the appendix by North Atlantic subregion, classification, index, and season.

The remaining sections focus on relationship with the NAO where the sensitivity of the blocking-NAO correlation to index and space were originally pursued in order to recreate portions of previous literature and ensure proper application of blocking indices. Area averaged bocking count and correlation with the NAO as in M13, W08, and Athanasiadis et al. (2020) were leveraged, revealing differences in results depending on index used. A full spatial correlation

by season, DB classification, and index is also provided for further context and understanding of the blocking-NAO relationship in the North Atlantic. Lastly, NAO terciles are introduced to determine how blocking event duration may differ given the phase of the NAO.

3.1 Blocking frequency

Figure 1 displays the resulting average blocking frequency by season from 1980 to 2019 from the 2D PV- θ blocking algorithm. The total frequency was classified into cyclonic or anticyclonic based on the DB values for day 0 or onset of each blocking event. Looking at the total frequency (first row of Fig. 1), common sectors with higher frequency for blocking emerge over the North Atlantic and Pacific such as

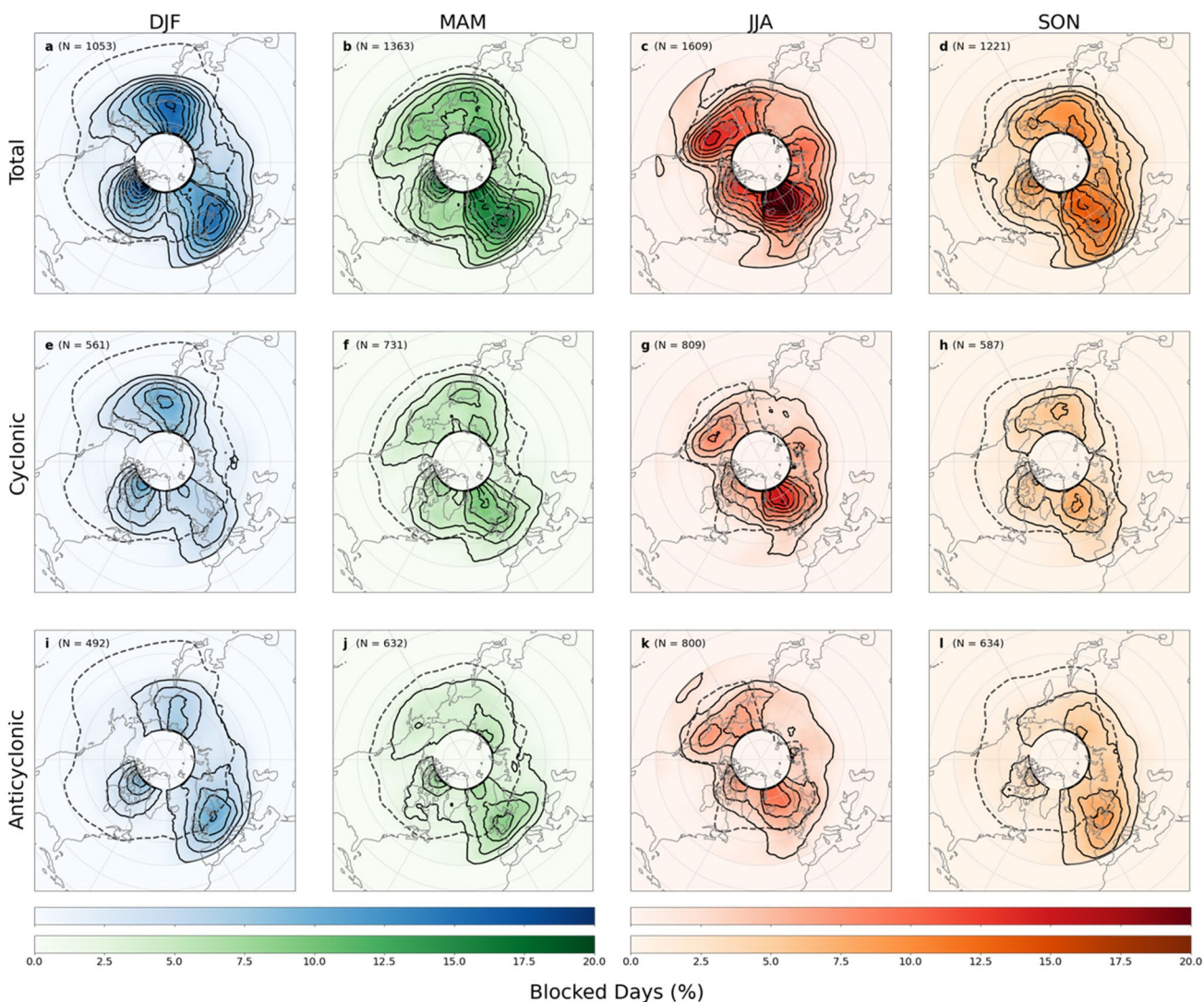


Fig. 1 Mean seasonal blocking frequency from 1980 to 2019 representing the average percent of blocked days per season in totality (a–d) and those driven by cyclonic (e–h) and anticyclonic (i–l) wave

breaking. Contours are every 0.02. N=number of total blocking events, over the 40-year study. The dashed line represents the CBL or seasonal climatology of maximum EKE by latitude

near Greenland, Europe, Alaska, Central-Western Pacific, and Siberia.

Considering the North Atlantic maxima over Europe and the West-Central North Atlantic (WCNA) during DJF, the first column of Fig. 1 shows that most of the wintertime WCNA blocking events are cyclonically driven while over Europe, anticyclonically. These maxima and their classification generally agree with the results found in M13, W08, and DV12 but with frequency values being slightly reduced. This could be attributed to the difference in study period and the addition of constraint to positive B values for a blocked day within the spatial limits of the tracking algorithm rather than all $B > 0$ considered globally or within a sector.

Following the seasonality of WCNA cyclonic blocking (second row of Fig. 1) the frequency maximum of ~10% in DJF decreases to ~6% in MAM and even more so to 4% in JJA, retracting northward to a much smaller spatial extent before extending further south in SON. Anticyclonic signatures are present over WCNA (last row of Fig. 1), reaching 8% in DJF, 6% in MAM and JJA, and 4% in SON only departing slightly in comparison to cyclonic blocking values suggesting that no one type of blocking truly dominates the WCNA region.

The European region displays more seasonality with the breaking type transitioning from mostly anticyclonic (~8%) in DJF to an overall maximum of ~16% of blocked days in JJA being driven cyclonically and ~8% anticyclonically. Comparing rows 2 and 3 of Fig. 1 over Northern Europe from DJF to MAM, the increase of cyclonic cases (~4% to ~10%) is matched with a gradual decrease in anticyclonic (~8% to ~6%), maintaining a similar spatial pattern. In JJA and SON the relative frequency of anticyclonic cases from MAM of ~6% is retained with only SON resembling DJF and MAM spatially as the JJA maxima retreats northward with the polar jet. Cyclonic cases over the region lower to ~6% in SON from their heightened values in MAM and JJA before returning to their DJF minimum (~4%).

Looking at the total frequencies (first row of Fig. 1), a pattern of propagation emerges over North Pacific regions from DJF to JJA with differences beginning in MAM and retreating in SON. Following the North Pacific-Eastern Asia DJF total maxima of ~14% (8% cyclonic, 6% anticyclonic) into MAM, the pattern becomes a lobe of two relative maxima—one slightly upstream near Siberia (~10% total) and the other downstream towards Alaska (~8% total). Figure 1c shows this transition further into JJA where a large total frequency of ~14% (~8% cyclonic, 6% anticyclonic) resides over Alaska and a new smaller max of ~8% (6% cyclonic, 2% anticyclonic) fully develops over Northcentral Asia. This maximum is somewhat retained during SON (~6%) while the Alaskan max dissipates more significantly (nearly 12%) as the transition into DJF begins.

Also plotted in Fig. 1 is the central blocking latitude (CBL; dashed line) derived from a seasonal climatology, rather than annual as in PH03. The CBL signifies the location of midlatitude weather systems which typically follow the subtropical and polar branches of the jet stream depending on the time of year and location (PH03, Berrisford et al. 2007). This is evident throughout Fig. 1 as the CBL retracts northward in the summer and generally follows the polar branch of the jet stream as mentioned in PH03. A CBL below blocking frequency maxima suggest that the jet is passing below the meridional θ reversal, and hence cyclonic breaking. A CBL above or through would suggest the jet is higher than the frequency maxima and hence anticyclonic breaking (Tyrlis and Hoskins 2008b). Indeed, the majority, if not all the cyclonic blocking frequency signatures are above the dashed line or follow it closely as do those over the Pacific regions. Anticyclonic blocking signatures, particularly over Europe tend to have the CBL pass through the maxima. The implications not only collaborate results here with that of Tyrlis and Hoskins (2008b) but also suggest high dependence of blocking results to the jet stream when applying the PV- θ index.

The seasonality of Fig. 1 provides classification across seasons and indicates that most differences in anticyclonic and cyclonic frequency by season are unique to region and largely follow the seasonality of the jet stream. While this is not a new finding by any means, a two-dimensional blocking frequency climatology across all seasons and classified by Rossby wave breaking is provided, updated through 2019. The next sections highlight the application of these classified blocking events to the blocking-NAO relationship.

3.2 Correlation with the North Atlantic Oscillation

3.2.1 Area averaged blocking

As previously discussed, the NAO and blocking have been heavily studied throughout the literature with their relationship strength commonly compared or leveraged through simple correlation analysis. To generate the blocking time-series correlated with the NAO, it is standard to compute the normalized area average blocking count for a given regional box. Both W08 and M13 follow this and used the PV- θ index to correlate the NAO and blocking count in the North Atlantic. Values of $r = -0.84$ unsmoothed, -0.93 smoothed and $r = -0.7$ were found, respectively. Athanasiadis et al. (2020), who used the AGP index, also found a strong anticorrelation between the NAO and high latitude blocking (HLB) over Greenland (-0.95) at extended, smoothed timescales. These correlation values have been strong enough to make just conclusion that the NAO and HLB (cyclonic blocking over Greenland) blocking are the

same phenomenon (W08) and even leverage NAO forecast skill to better predict blocking (Athanasiadis et al. 2020).

Replicating these correlation values were attempted but not fully achieved with similar application of the PV- θ and AGP indices here. High correlation values were found with the AGP index, though, with the PV- θ index they were not. Multiple attempts to locate high correlation values with the PV- θ index and the NAO were made, choosing various North Atlantic regions for blocking, only considering cyclonically driven blocks as in M13 and as suggested by W08, or where blocking frequency maxima occur.

Regardless of test performed, the correlation of wintertime NAO and cyclonically driven blocks/those over the Greenland region were significantly lower (~ 0.01 to 0.5) to previous work (W08, M13) and displayed pronounced sensitivity to the exact region chosen to average blocking count.

In Fig. 2, one example of the area averaged normalized DJF blocking count and NAO correlation tests is presented with both the AGP and PV- θ indices along one another. The region chosen was 55° – 75° N, 0° – 80° W (red box Fig. 2a, b), estimated from that used in Athanasiadis et al. (2020) and chosen to show the relationship of Greenland blocking/HLB

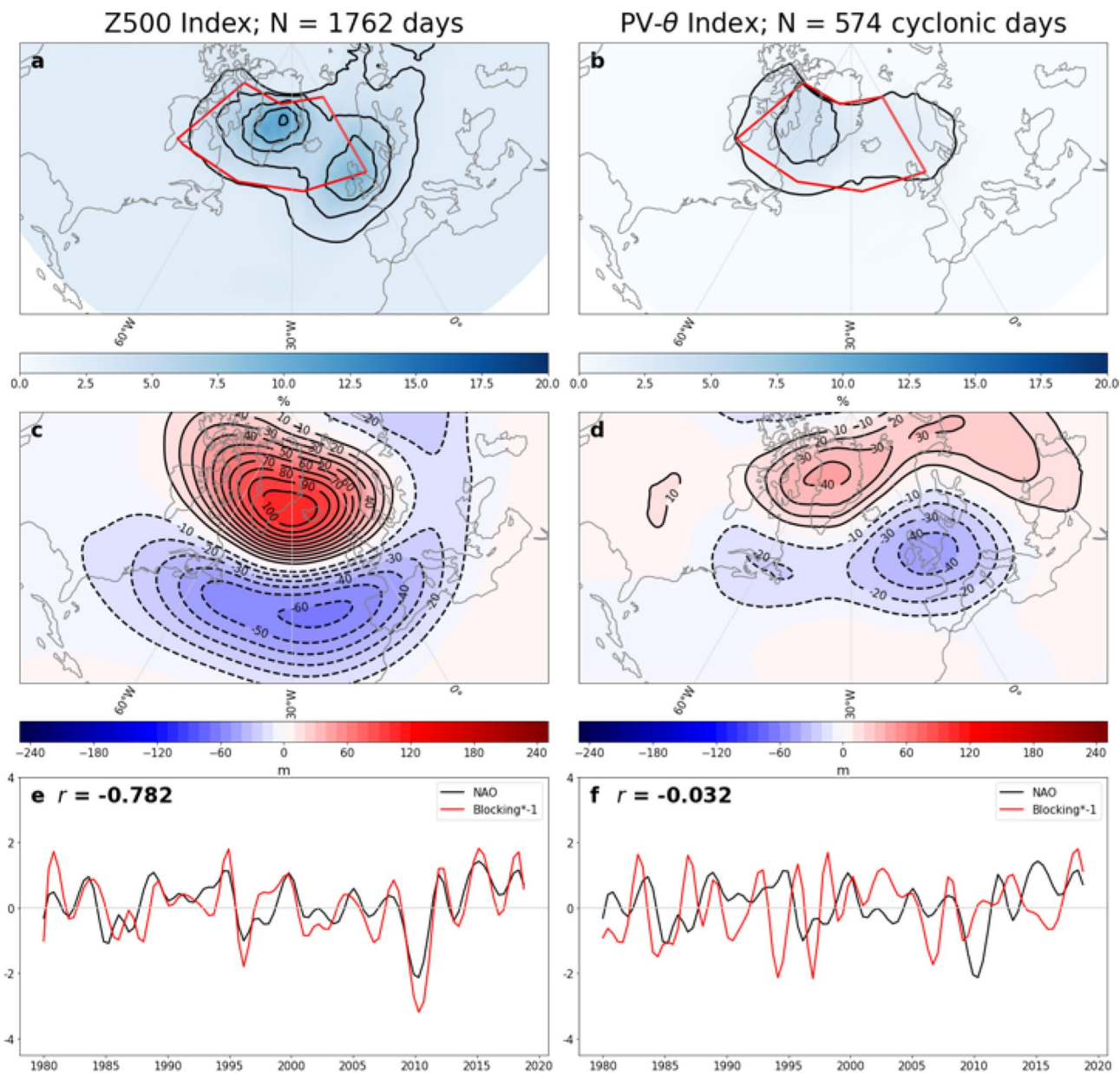


Fig. 2 a, b Blocking frequency, c, d daily 500mb geopotential height composites and e, f correlation of the normalized blocking count with the NAO over the region 55° – 75° N, 0° – 80° W derived by the a, c, e

AGP index and b, d, f PV- θ index, considering only cyclonic cases. Note the blocking timeseries in e, f were multiplied by -1 to better represent the anti-correlation values in the upper left corner

and cyclonic blocking over the North Atlantic. Further, an example of only cyclonic blocking is used as it is cited as being used for correlation in M13 and the cause of HLB over Greenland in W08. Though, total (unclassified/both cyclonic and anticyclonic) blocking events or considering only anticyclonic cases does not alter the result of low correlation of area averaged blocking count and NAO index that can be seen in Fig. 2e, f. It is shown that regardless of the blocking count and classification, the correlation between DJF blocking and the NAO remains small when using the PV- θ index over the regions provided by Athanasiadis et al. (2020) and W08.

The timeseries in the bottom panels of Fig. 2e, f represent normalized blocked day count by season so even though the averaged blocking frequencies are of similar magnitude (Fig. 2a, b), the number of days considered blocked are differing from year to year between indices. This is directly visible in the timeseries and supported by the 500 mb geopotential height anomaly composite for all blocked days considered (Fig. 2c, d). The Z500mb composite for AGP blocks is more intense and resemble more closely a typical NAO dipole structure. The PV- θ cyclonic blocking composite is weaker with two negative lobe patches rather than the large, negative AGP swath. It can be concluded from Fig. 2b–f that different blocking events are being measured between the two indices, driving the stark difference in correlation value.

Why is this? Does it have to do with the vertical structure or height of the 2PVU surface differing from the 500 mb level? Are the indices picking up on different portions of the flow field and classifying them as blocks? Is it a threshold problem where the reversal criteria are not met for a given index? While the answer to these questions is not directly within the scope of this paper and were unable to be answered with the analysis performed here, attention will once again be brought to the results of Pinheiro et al. (2019). In their 2-D index comparison study, it was found that AGP blocks differed the most overall from Z* and PV* indices with sensitivity of AGP detection to threshold. Further, they found the PV* index used would at times pick up on jet streaks, misidentifying blocks and leading to differences with the other indices.

Overall, both methods have their caveats on what they detect and subsequently, following one of the larger results from Pinheiro et al. (2019), correlating blocking events spatially to other phenomenon will lead to different results depending on the index used. Ultimately this is being seen here with blocking and the NAO, likely resulting from both a threshold (AGP) and misidentification (PV- θ) problem. This yields a cautionary result for studying the likeness of these two phenomena in the North Atlantic based on index chosen and the area considered for comparison, differing from the consensus that HLB/Greenland blocking events and the NAO are the same thing (Athanasiadis et al. 2020; W08).

3.2.2 North Atlantic wide spatial correlation

While the exact reasoning as to why the two indices differ in area average correlation is not provided, a closer look at the correlation between blocking and the NAO is. Figure 3 shows a full, 2-D, grid point spatial correlation—removing sensitivity of area averages—by index, DB-classification, and season. Considering first the results of DJF cases (first column of Fig. 3) three conclusions can be drawn from the PV- θ cyclonic (Fig. 3a), PV- θ anticyclonic (Fig. 3e), and AGP (Fig. 3i) analysis. The first is that there is no major, significant correlation with wintertime NAO and anticyclonic blocking cases (Fig. 3e).

The second is that there is a significant ($p < 0.05$) anticorrelation with DJF PV- θ cyclonic blocking cases spanning most of 90°W–0°E in the range of $r = -0.40$ to -0.55 . A local maximum near 30°W of -0.76 is also obtained, confirming the work of M13 stating a correlation of -0.7 with cyclonic blocking and NAO. It also somewhat validates the work of W08 ($r = -0.84$ unsmoothed, -0.93 smoothed) for HLB blocking. This small region, however, is much farther east than the work of W08 who purposely excluded blocks east of 30°W to omit European events. Even though the same index is used, a large difference between this study and W08 is present and could be arising from that fact that our 40-year study period is shifted ~ 20 years later than their 1957–2001.

The implication of this difference follows a noted eastward shift in wintertime NAO centers of variability between two periods: P1: 1958–77 and P2: 1978–97 in a study by Jung et al. (2003). One proposed mechanism was a difference in strength of the background westerly flow during P2, a theory later confirmed by Luo and Gong (2006) using a nonlinear barotropic model. The relevance here is that P1, the period of largely westward NAO, is mostly excluded in our study whereas P2, the predominately eastward NAO, is included. The additional, later and warmer 20-year period presented here, showing eastward relational trend, weakly supports results of Ulbrich and Christoph (1999) and notion of this shift being attributable to rising greenhouse gas forcing and consequential strengthening of the wintertime storm track. Though, with only a presented eastward shift in the blocking-NAO correlation and without direct consideration of the role of warming in our analysis, attribution of the difference in our results to W08 to greenhouse gas induced variability cannot be concluded and warrants further study.

It is more reasonable to support yet another cautionary result in the literature from Jung et al. (2003) who stated basing conclusions using long-term NAO, due to strong interannual variability, should be taken with care, particularly at short (20-year) timescales. Interannual variability of both the NAO and blocking is hypothesized to be the reason for differences between results here and with W08. It can

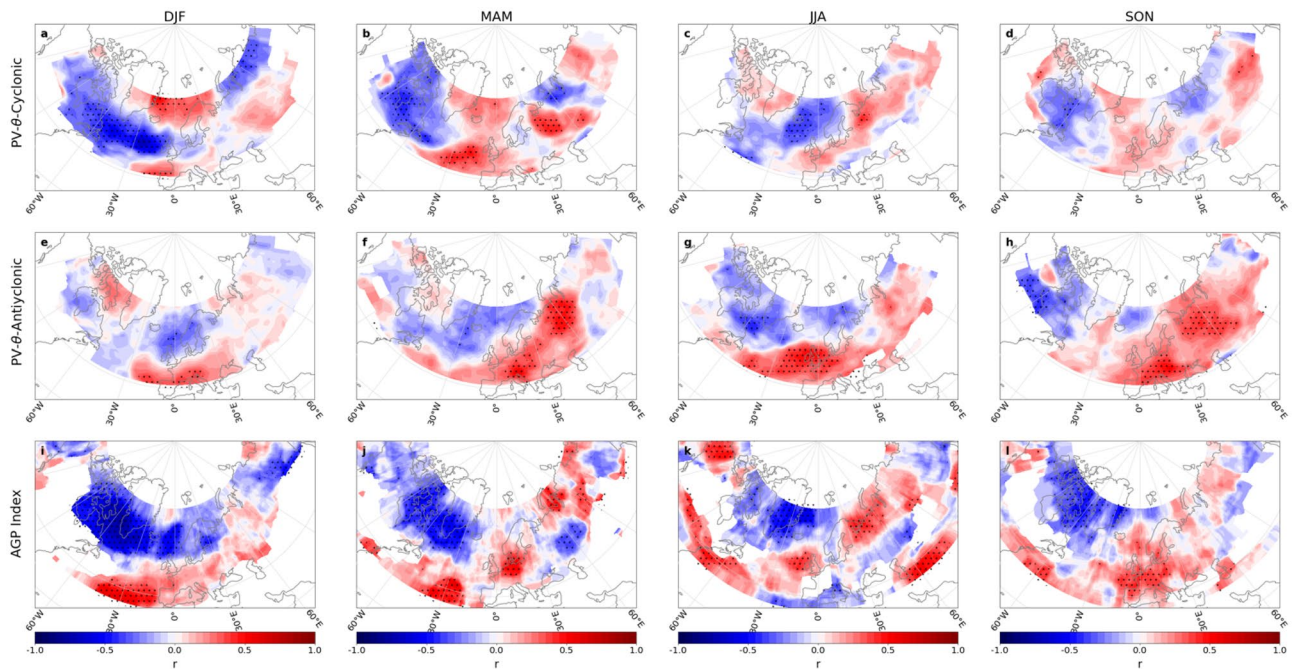


Fig. 3 Spatial correlation (shading) of the seasonal North Atlantic Oscillation index with cyclonically **a–d** and anticyclonically **e–h** driven normalized blocked days derived from the PV- θ index and **i–l**

from the AGP index by season from 1980 to 2019 across all seasons in the North Atlantic sector. Stippling denotes significance from a student's t test for $p < 0.05$

be further asserted from Fig. 3 and the work of W08, Jung et al. (2003), and Luo and Gong (2006) another sensitivity of blocking-NAO analysis to the study period chosen.

The third and last conclusion from the first column of Fig. 3, DJF cases, extends results from Fig. 31 of sensitivity of the NAO-blocking correlation to index chosen from area averages to the full region. In Fig. 3i, there is a larger swath of higher, more spatially consistent anti-correlation values stretching from 90°W – 0°E when applying the AGP index compared to values derived from the PV- θ index (Fig. 3a, e). Further, this region of 20% higher correlation values is displaced 30°W and 10° – 20°N of the PV- θ cyclonic maximum. This northwestward shift in the maximum range of the AGP results somewhat contradict the results from the PV- θ index based on the eastward shift discussed above. The same reasoning does not apply to both indices as the AGP results do not present an eastward shifted maximum. This stresses the differences in results and conclusions of blocking analysis based on index chosen. It also could be reinforcing that each index is picking up on different blocking events.

Considering the other seasons, the correlation of NA blocking and the NAO display variability that largely resembles jet stream variability. This is particularly true for cyclonic and anticyclonic PV- θ cases (Fig. 3a–h), echoing locations of respective blocking frequency in Fig. 1, but also seen in AGP results (Fig. 3i–l). With exception to DJF, the remaining seasons develop a largely negative west, positive

east correlation pattern seen throughout cyclonic, anticyclonic, and AGP cases from MAM to SON (Fig. 3b–d, f–h, j–l). This pattern is most prominent anticyclonic cases in MAM and SON where anticyclonic blocking and NAO+ correlate strongly and significantly ($p < 0.05$, Fig. 3f, h). Further, and interestingly, the pattern at times does take on a negative north, positive south structure as in DJF and JJA anticyclonic cases.

Overall, the implication of Figs. 2 and 3 suggests that when considering the relationship of North Atlantic atmospheric blocking and the NAO, the type of index, exact region, season, and study period should be considered. These results are consistent with Scherrer et al. (2006) who showed high sensitivity of the NAO/NA blocking correlation to latitude–longitude and varying indices during DJF. The spatial correlations derived from the PV- θ index and their differences with the AGP index also support the notion from Pinheiro et al. (2019) that correlating blocking events spatially to other phenomenon such as extreme weather will lead to different results depending on the index used. This is stressed in the discussion on the location of the blocking-NAO correlation center being eastward (PV- θ cyclonic) or northwestward (AGP). Relying solely on the AGP index could lead to a missed opportunity of how both the NAO and blocking are changing with additional 20-year periods as presented here, carrying large implications for generalizations made on the NAO, NA blocking, and both

short and long-term weather and climate prediction. However, the AGP index has reproduced consistent and strong correlation values suggesting it could be more useful than the PV- θ index for correlation analysis. These implications are explored further in the next section where all blocking analysis sensitivities are displayed through impacts on weather variables such as precipitation, via composites across all seasons.

3.3 Blocking duration

The previous sections discuss blocking and how several analysis techniques lead to varying results when applied to the blocking-NAO. But what about blocking itself? How can the identified analysis sensitivities translate to useful information about blocking, not just blocking analysis? This section aims to answer this question by considering blocking duration and how that may change given the region, index, classification, and NAO phase. Further, by studying which NAO tercile the block formed in and how that may relate to duration, the blocking-NAO relationship moves beyond whether they are the same and to what degree, into more applicable information. Duration based on NAO tercile at onset was chosen based on previous discussion of potential differences between the AGP and PV- θ index criteria for blocking onset. The results are shown in Figs. 6, 7, 8, with each representing a different North Atlantic subregion from Fig. 4 and each panel a season. Note that the y-axis does

shift per figure. NAO terciles and the distributions they were determined from are provided in Fig. 5.

Most of the boxplots show a positive skew, following typical blocking duration distribution rapidly declining in likelihood with increased duration. The Ural and Greenland (Figs. 6, 8) regions have the shortest duration range values, increasing over the European sector (Fig. 6). All regions have medians, regardless of season, averaging between 6–7 days. The highest overall median durations occur with AGP blocks during the upper NAO tercile for DJF Ural blocks and MAM European blocks (Figs. 6a, 7b).

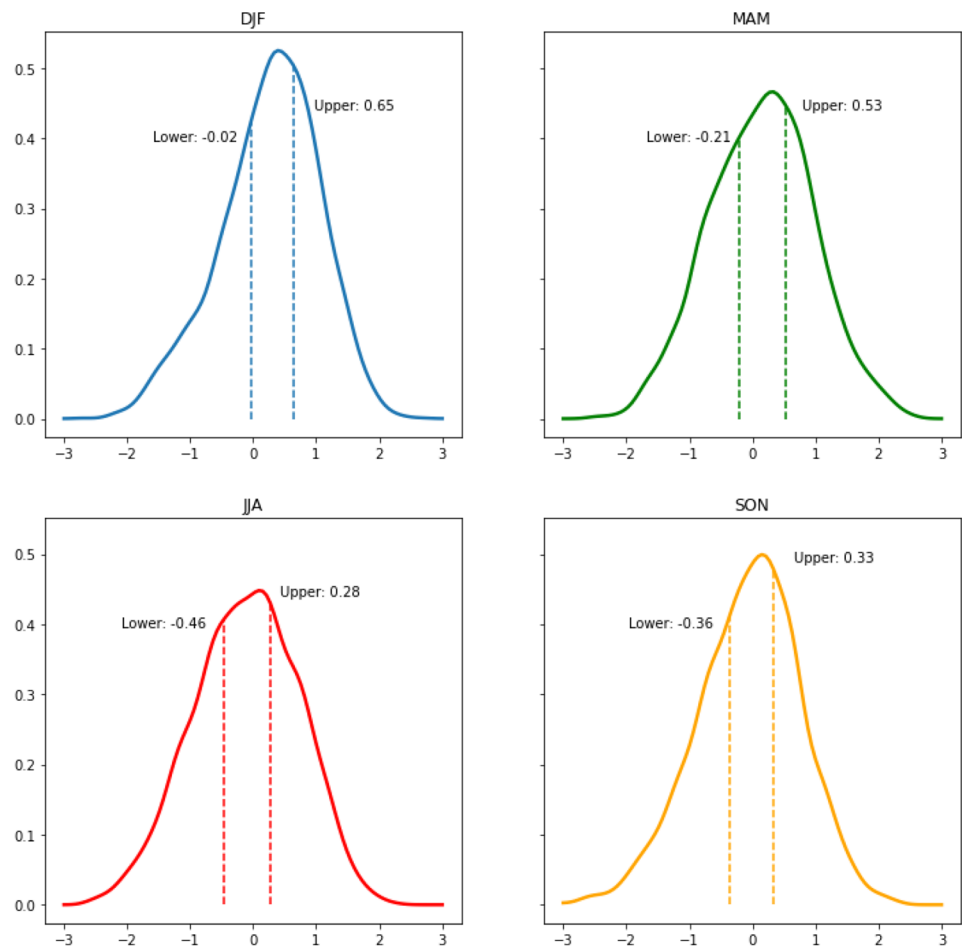
Cyclonic PV- θ blocking tends to be the shortest lived throughout, with only slight upticks in range for the upper tercile of NAO days and are typically highest during MAM and JJA, consistent with the blocking frequency results in Fig. 1. Anticyclonic PV- θ has higher ranges over the European region but are fairly consistent throughout with only some standout features such as a larger shift in JJA lower tercile range over Europe (Fig. 7c).

AGP results have the largest duration range regardless of the region, season, and NAO phase, displaying more sensitivity than the PV- θ cases. This supports the argument, paired with the lower, outlier filled PV- θ values, that only more intense, longer lived blocked are picked up by the AGP index compared to the shorted lived PV- θ , noisier blocks. This is also displayed through the lack of AGP representation across all terciles for most of Ural and Greenland blocks (Figs. 6, 8).



Fig. 4 Atlantic sub-regions selected for blocking duration analysis

Fig. 5 The distribution of daily NAO index for each season from 1980 to 2019 with resulting tercile ranges used for duration analysis.



PV- θ cases mostly do not favor one tercile over the other whereas the majority of AGP blocks fall into two of three NAO phases. Is this due to the lack of AGP threshold criteria or more attributable to the allowance of PV- θ blocks to have slight movement across the region? The duration plots support the argument that the PV- θ index could be better for analysis of blocking onset and AGP for more established, anomalous events.

Regarding useful information relating the duration of blocks to NAO phase, there is no real conclusion to be made as the results show general consistency for blocking duration with only slight sensitivity between season and region. However, for most cases, blocking onset occurs during all NAO phases, regardless of region, season, and index used. Specifically for cyclonic and anticyclonic PV- θ blocks, no one NAO phase dominates duration or onset occurrence. Further, this analysis provides an example of how, beyond composites, multiple techniques could

be useful in gaining a full picture of blocking and how it relates to other phenomena.

4 Summary and conclusions

While blocking index comparisons, climatological studies, and blocking-NAO have all been heavily cited throughout the literature, the primary goal of this study is to specifically show how choice of blocking index leads to varying results in the strength of the blocking-NAO relationship. The methodological approach follows a 2-D PV- θ index curated in Masato et al. (2011) from December 1979 to November 2019 paired with a complimentary direction of breaking (DB) index (Masato et al. 2011). The DB metric measures the direction of Rossby wave breaking associated with the onset of blocking events as either cyclonic or anticyclonic and classifies them as such. The second index,

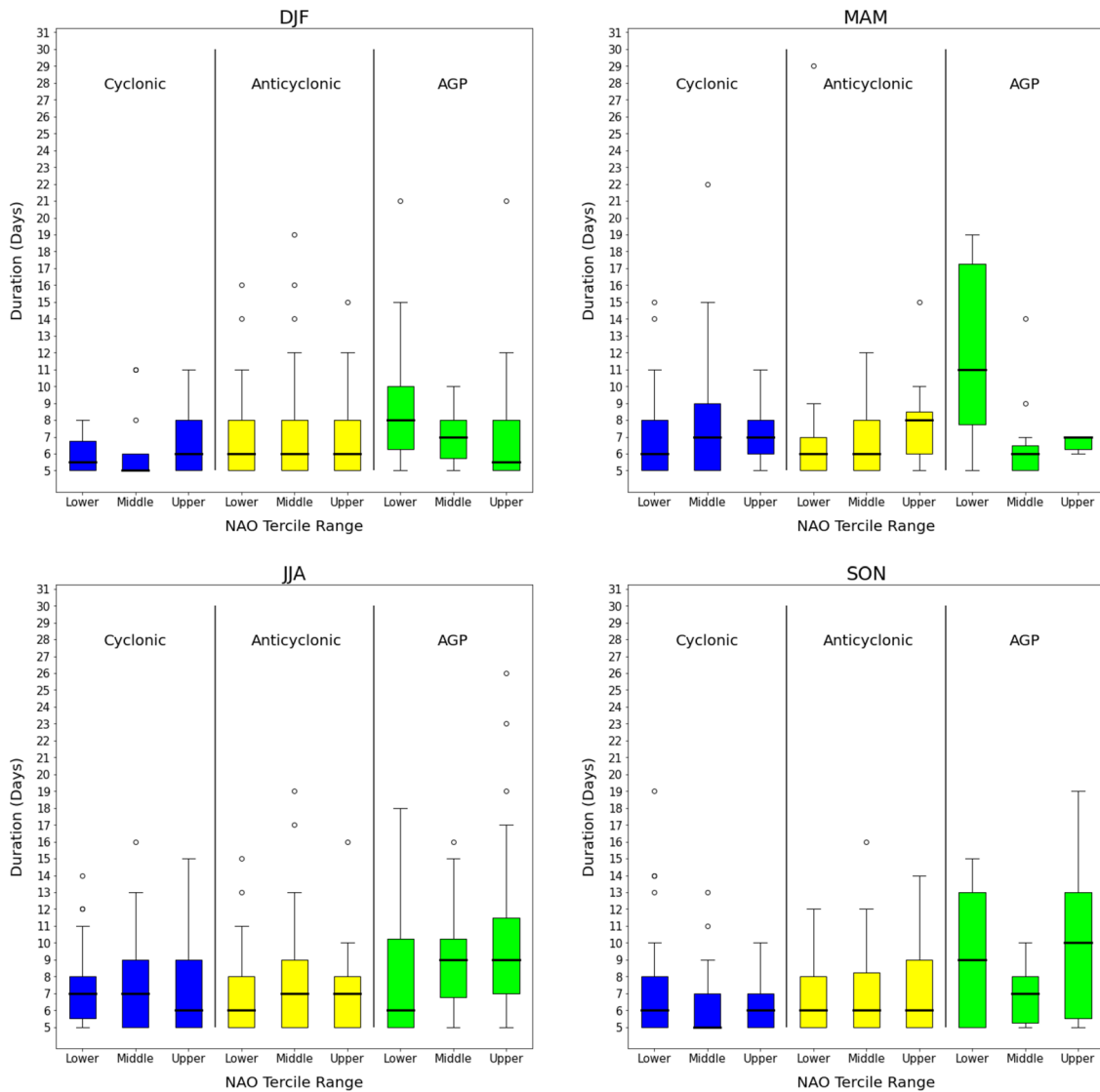


Fig. 6 The duration of blocking events by AGP and classified PV- θ index produced blocking events by season for the Ural North Atlantic subregion based on the NAO tercile at blocking onset

a common 2-D 500mb geopotential height index (hereafter referred to as the AGP index; Davini et al. 2012) is used to compare the results developed with the PV- θ index here as well as against previous literature.

Although extensive work exists on blocking climatology and associated impacts of blocking events, a comprehensive and updated (through 2019) North Atlantic blocking climatology produced by the PV- θ index with DB classification is still included in this work for context, comparison with other studies, and future reference.

In the main text, a 40-year blocking climatology of PV- θ classified Northern Hemispheric blocking across all seasons is provided. In the appendix, composite anomalies of

various weather-related variables such as sea surface temperatures and precipitation during blocking events are presented alongside NAO composites in the appendix by North Atlantic subregion, classification, index, across all seasons.

The results of the PV- θ frequency analysis, in agreement with previous work, show there is a higher amount of DJF anticyclonic blocking over Europe than cyclonic blocking (Masato et al. 2011, 2013; Woollings 2008; Davini et al. 2012). However, the average anticyclonic blocking frequency over Europe is near equivalent to its frequency over western Greenland. Further, the maximum blocking frequency approaches 24% over northwestern Europe during JJA, two thirds of which is contributed by cyclonic

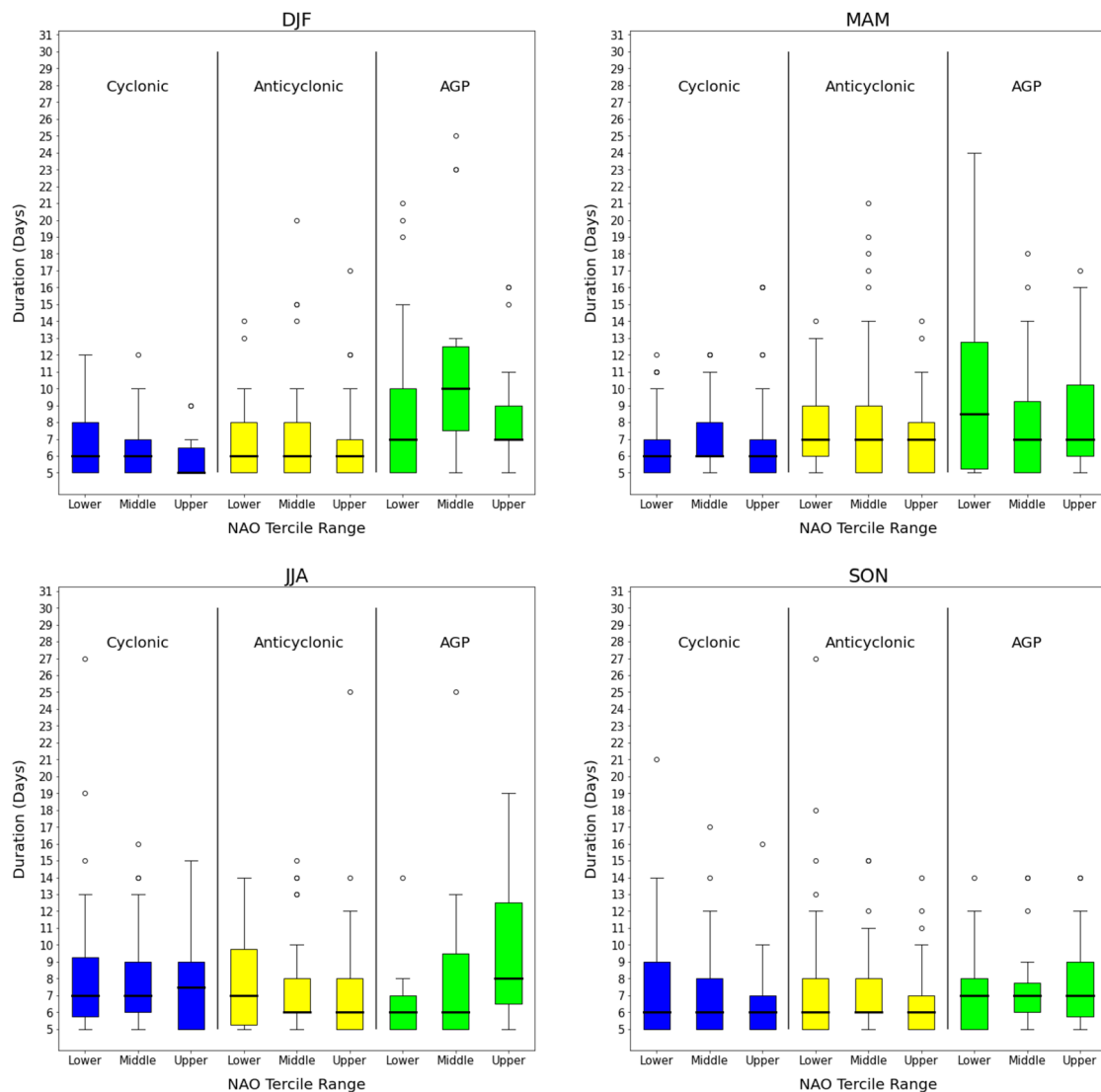


Fig. 7 The same as Fig. 13 but for the European region considering the duration of AGP and classified PV- θ blocking events by season during NAO tercile

blocking. MAM and SON display frequencies in between but relatively similar to DJF and JJA and generally follow the seasonality of the jet stream. Lastly, the climatological blocking frequency values produced by the PV- θ index are considerably higher than to the AGP index (see Appendix), on the order of ~ 15 to 20%.

The difference between indices can further be seen in the attempting to relate wintertime area averaged blocking count and the NAO. It can be concluded that different blocking events are being measured between the two indices, leading to stark differences in the NAO correlation. Those found with the AGP index result in a nearly identical composite of

NAO- whereas the PV- θ cyclonic case is weaker and less pronounced. Further, the correlation values found with the PV- θ index in the area averaged analysis are dramatically lower than the AGP and previous work (Athanasiadis et al. 2020; Masato et al. 2013; Woollings et al. 2008).

To better understand the full scope of the blocking-NAO correlation in the North Atlantic and to the spatial sensitivity of the correlation, a spatial grid-point analysis across all seasons was also presented. Here four general conclusions can be made: first, correlating normalized blocking count over the Atlantic with the NAO reveals a distinct seasonality that gradually forms a zonal asymmetry of negative west/

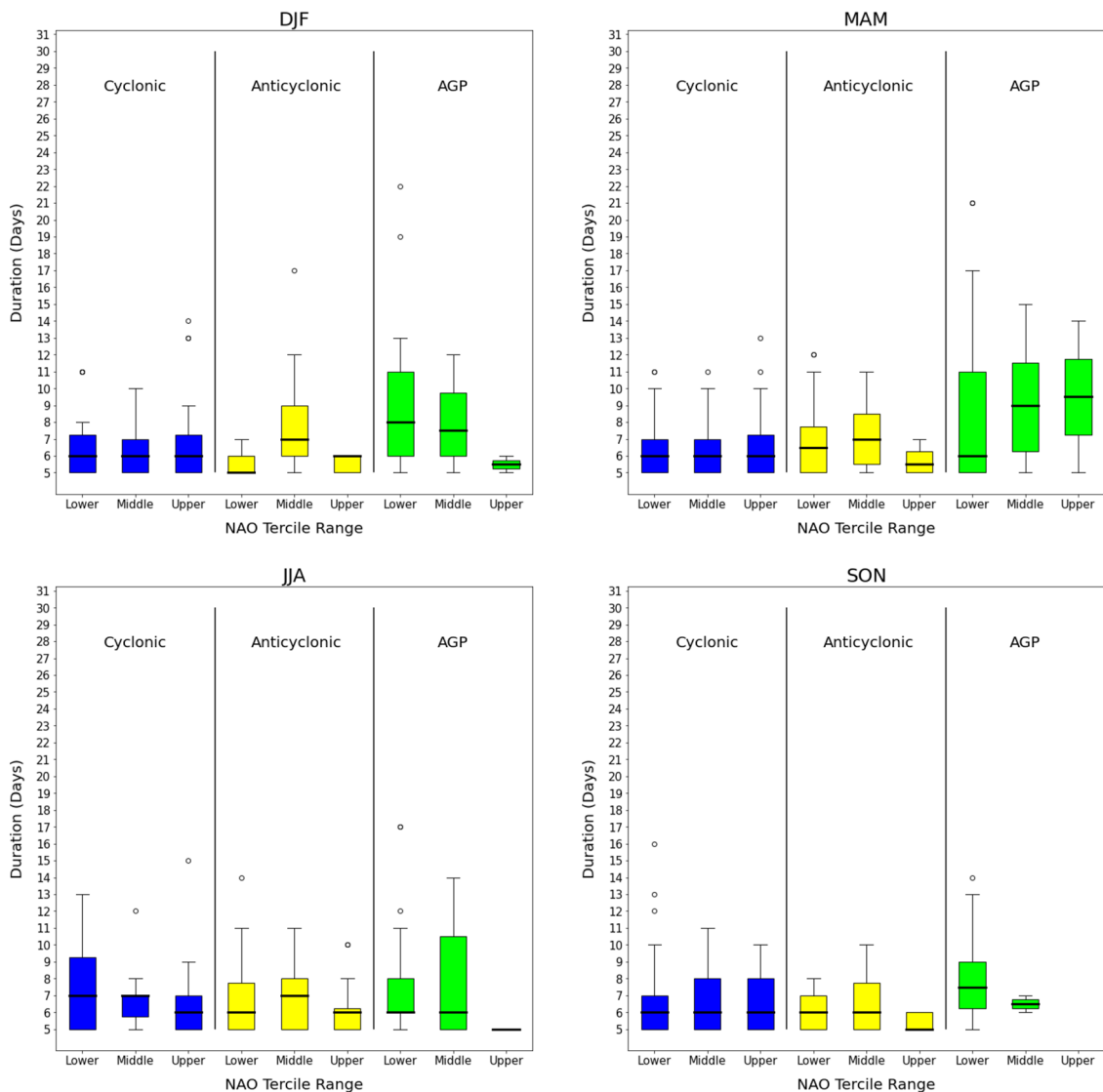


Fig. 8 The same as Fig. 13 but for the Greenland region considering the duration of AGP and classified PV- θ blocking events by season during NAO tercile

positive east, also seen in Scherrer et al. (2006) but for DJF only. However, the DJF pattern is the only season that does not display the zonal pattern, but rather a meridional structure east of 30°W with negative correlations to the north and positive to the south.

Second, there is no major, significant correlation with wintertime NAO and anticyclonic blocking cases. Third, a prominent sensitivity of the NAO-blocking correlation to index chosen is present for both area averages and the full region as AGP DJF correlations span a large swath of significantly higher correlation values, northwest of the PV- θ

cyclonic max. While blocking index sensitivities are known, application of this specifically to the NAO-Blocking correlation is new here.

And fourth, there is a significant, yet moderate anti-correlation with DJF PV- θ cyclonic blocking cases but shifted southeastward from the even stronger swath of high values found with the AGP index. The ‘noisier’ PV- θ allowed for a potential eastward shifted signal to be captured in the North Atlantic wide NAO-blocking correlation that was otherwise missed by the AGP index. Compared to other studies who performed similar analysis—with a study

period shifted 20-years prior—the maximum correlation of cyclonic blocking over Greenland found here is 30°E of theirs (Athanasiadis et al. 2020, Woollings et al. 2008). While this likely reflects the interannual variability of both the NAO and blocking, it does bring the cautionary result that cyclonic blocking over Greenland and the NAO may not be as strongly correlated as previously believed. This warrants further study, especially with the potential implications of how differing decades may be changing the relationship into the future.

Blocking event duration by NAO tercile were considered to try and dissect any further relationship between cyclonic, anticyclonic, and AGP blocks and the NAO. While the overall results did not yield specific information on any standout durations. It can be concluded, for the majority of cases, blocking onset occurs during all NAO phases, regardless of region, season, and index used. Specifically for cyclonic and anticyclonic PV- θ blocks, no one NAO phase dominates duration or onset occurrence. However, it was revealed that AGP blocks displayed the largest spread in duration.

Combining frequency, duration, and supplemental composite analysis (see Appendix), a hypothesis as to why the differences between the indices are emerging. The PV- θ index results are more frequent, shorter in duration, correlate less with wintertime NAO over Greenland, and appear in composite analysis more as features of the larger scale planetary flow. In converse, the AGP index is near opposite the PV- θ index and displays large, more standout anomaly signals in the composite analysis and near identical to the NAO- composite across all seasons. It is thus felt that the AGP index is identifying more traditional, higher end of the distribution, mature, or ‘canonical’ blocking events. Whereas the PV- θ blocks represent noisier, less ‘perfect’, Rossby wave-driven meridional reversals that meet spatial and temporal constraint of blocking. Relating back to the nuances of the index application and further supporting the argument, the AGP index requires the meridional reversal to meet a threshold criterion before being considered a blocking event. The PV- θ index begins counting towards temporal constraint once a meridional reversal is detected and being stored as blocking event if that reversal is large and persistent enough.

This can further explain the stark difference seen in the Greenland blocking-NAO correlation between the indices. Larger, more persistent and mature blocking structures over the North Atlantic are more likely to coincide with what

constitutes the NAO, particularly those over the Greenland region and NAO-, having greater influence on sea level pressure variability for extended periods. A lower end noisier PV- θ index reversal event would, in theory and shown in correlation values here, be less likely to have a spatial-temporal overlap with a more traditional NAO- dipole structure over Greenland.

The results here suggest that the lack of consistency in blocking methodology and what is defined as blocking events could be contributing to some of the discrepancies found in blocking-NAO related variability over the North Atlantic. Shown here, choice of blocking index alone leads could lead to Greenland blocking and NAO- appearing the same, sometimes the same, or not the same phenomenon consistent with the myriad work on the relationship of the two (Woollings et al. 2008; Athanasiadis et al. 2020; Croci-Maspoli et al. 2007; Yao and Luo 2018; Shabbar et al. 2001; Scherrer et al. 2006).

While the use of additional multiple indices may be presented as a disadvantage, there are benefits to considering the application of both the AGP and PV- θ , even within the context of the NAO. The AGP index, with resulting ‘canonical’ blocks, is recommended to be more reliable for correlation and extreme event analysis than the PV- θ cases as well as for relating to seasonal to longer term NAO signals. The PV- θ index provides better context for what is driving the onset of blocking events such as planetary wave sources, revealing how lower-end, short lived blocking events could be changing in the future, and help connect Rossby wave breaking dynamics shared by both blocking and the NAO (Benedict et al. 2004). One index is not better than the other, though, the indices we are applying to blocking related problems should be more carefully considered.

Ultimately, a more consistent methodology that captures multiple blocking forms, such as proposed by Sousa et al. (2021), would be more useful and is encouraged for future works. By applying their conceptual model, for example, one may be able to fully distinguish the actual type of blocking structure that overlaps with NAO-, potentially revealing a better understanding on the relationship of the two.

Appendix

Figures 9, 10, 11, 12, 13, 14, 15, 16 and 17.

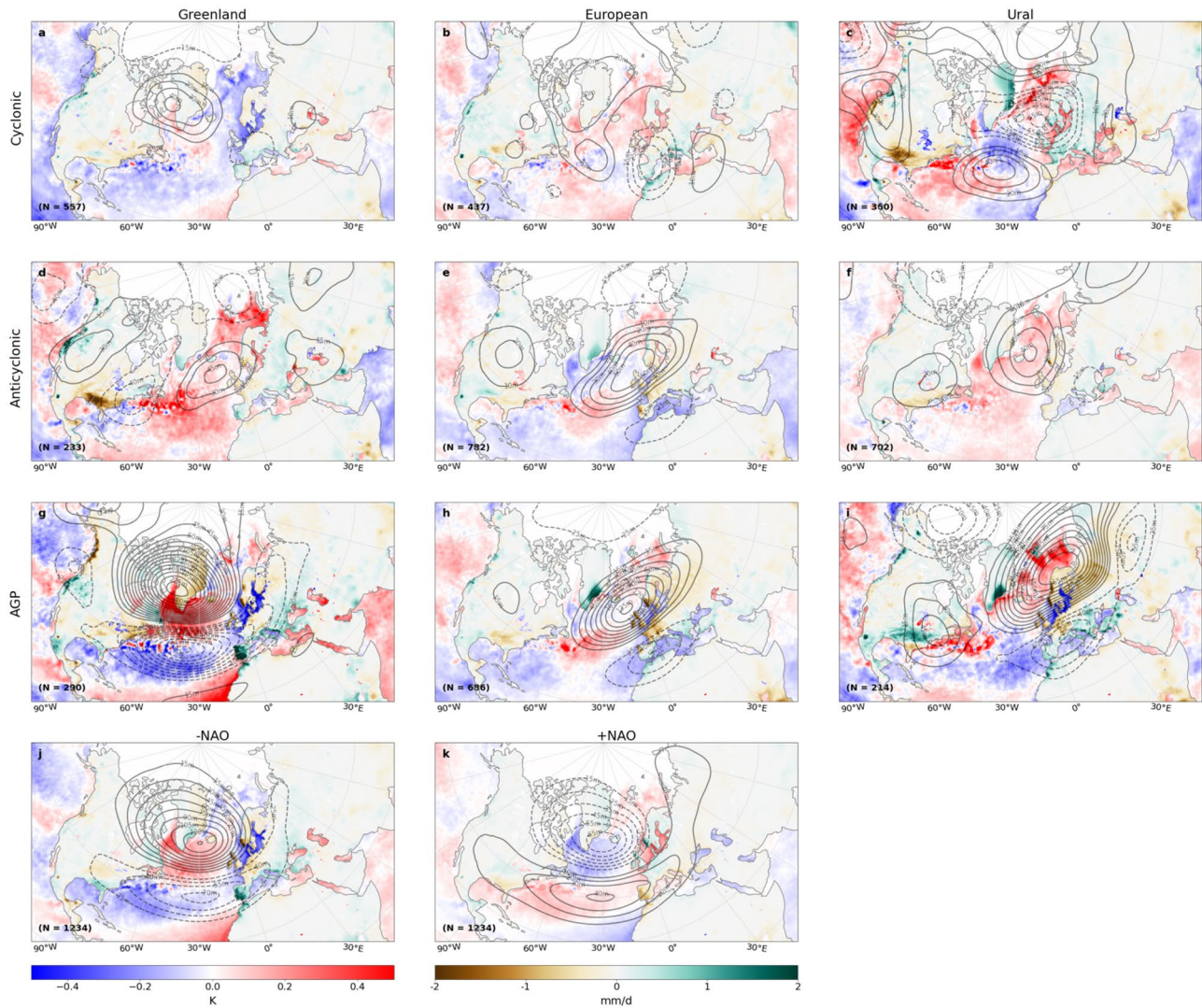


Fig. 9 DJF composites of anomalous Z500mb (black contours), precipitation (brown-green shading), and SSTs (blue-red shading) during all blocked days within a given subregion, by index and for the PV- θ blocks, by classification. Classified cyclonic PV- θ blocks by

the Greenland, European, and Ural regions are in panels **a–c**, **d–f** for PV- θ anticyclonic blocks by subregion, and **g**, **h** for AGP blocks. Daily NAO composites are also provided for context and comparison in **(k)**. N represented the number of days included in the composite

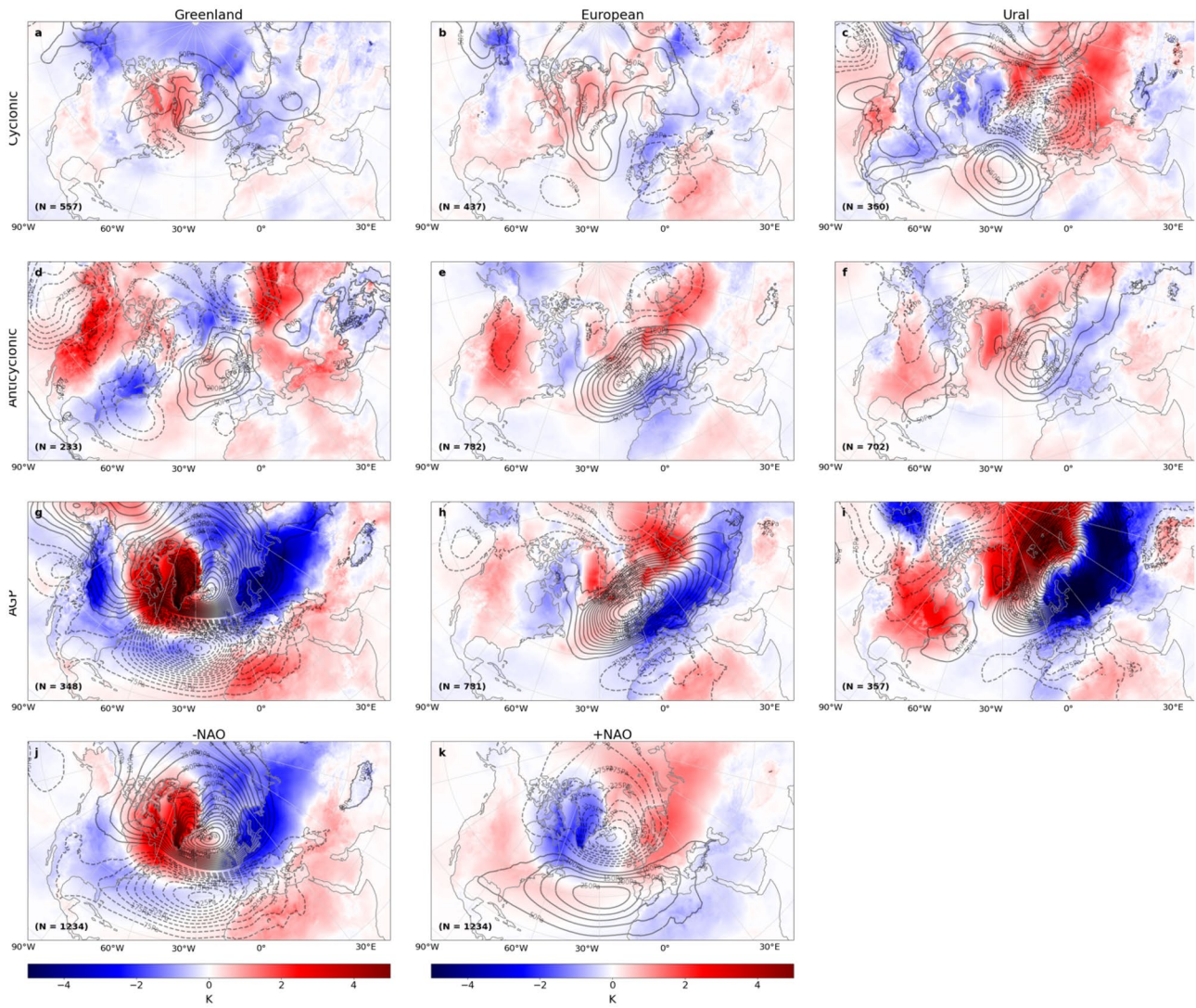


Fig. 10 The same as Fig. 9 showing daily blocking event and NAO composites by subregion and index during DJF, but for anomalous sea level pressure (contours) and two-meter temperature (blue-red shading). Contours are every 50 mb

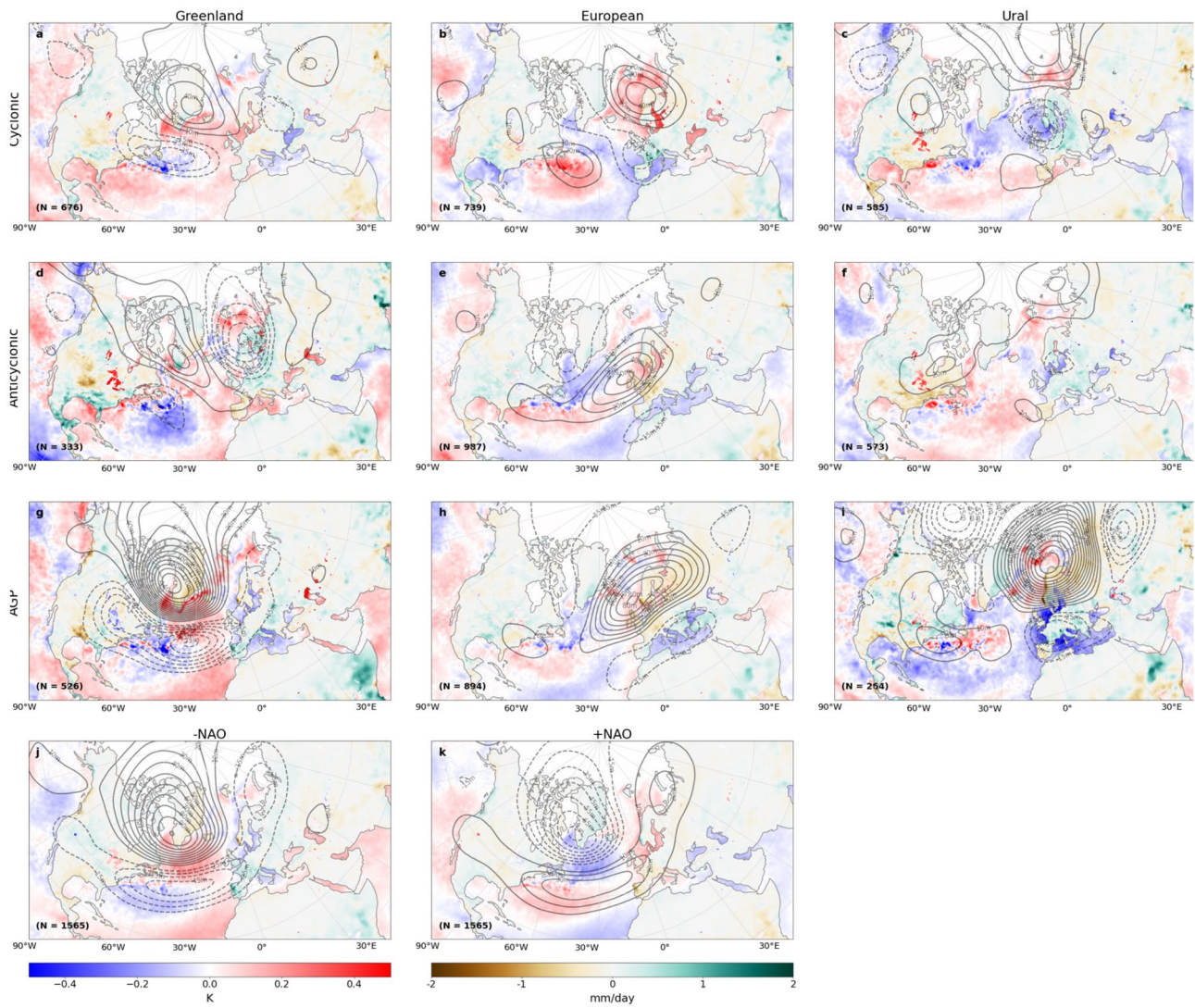


Fig. 11 the same as Fig. 9 but for MAM, showing daily blocking event and NAO composites by subregion and index of anomalous Z500mb (black contours), precipitation (brown-green shading), and SSTs (blue-red shading)

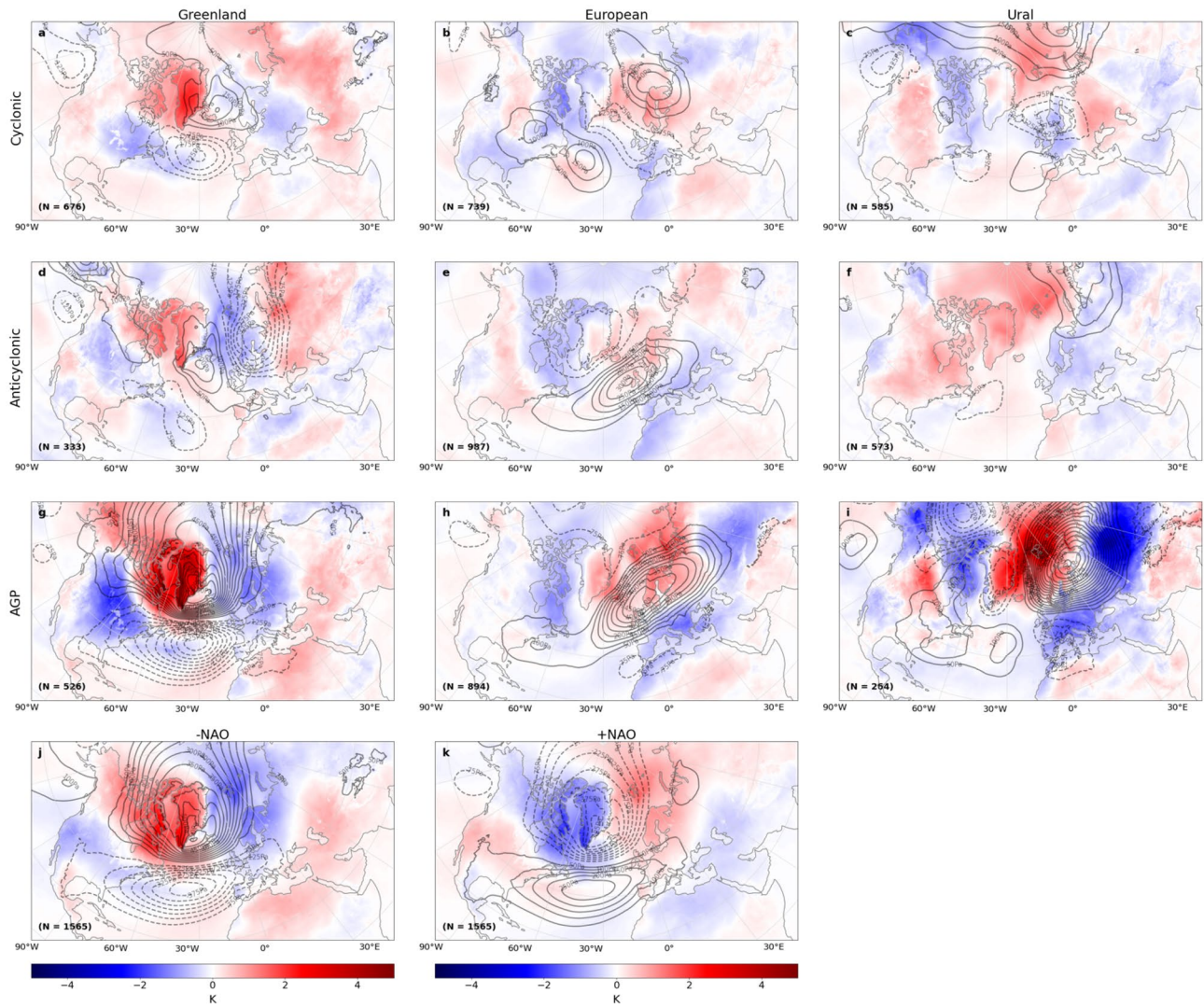


Fig. 12 The same as Fig. 10 but for MAM, showing daily blocking event and NAO composites by subregion and index for anomalous sea level pressure (contours) and two-meter temperature (blue-red shading). Contours are every 50 mb

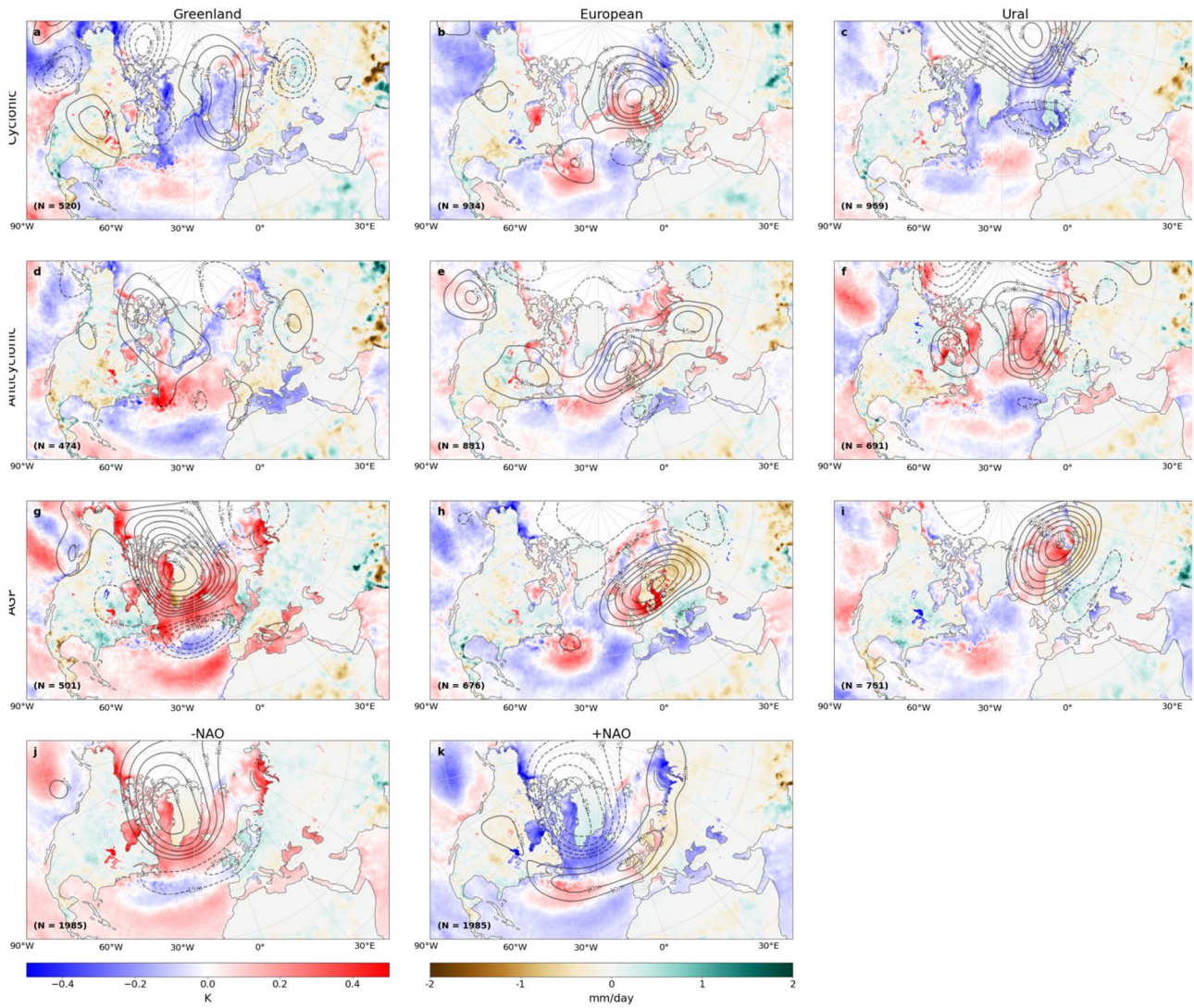


Fig. 13 The same as Figs. 9 and 11 but for JJA showing daily blocking event and NAO composites by subregion and index of anomalous Z500mb (black contours), precipitation (brown-green shading), and SSTs (blue-red shading)

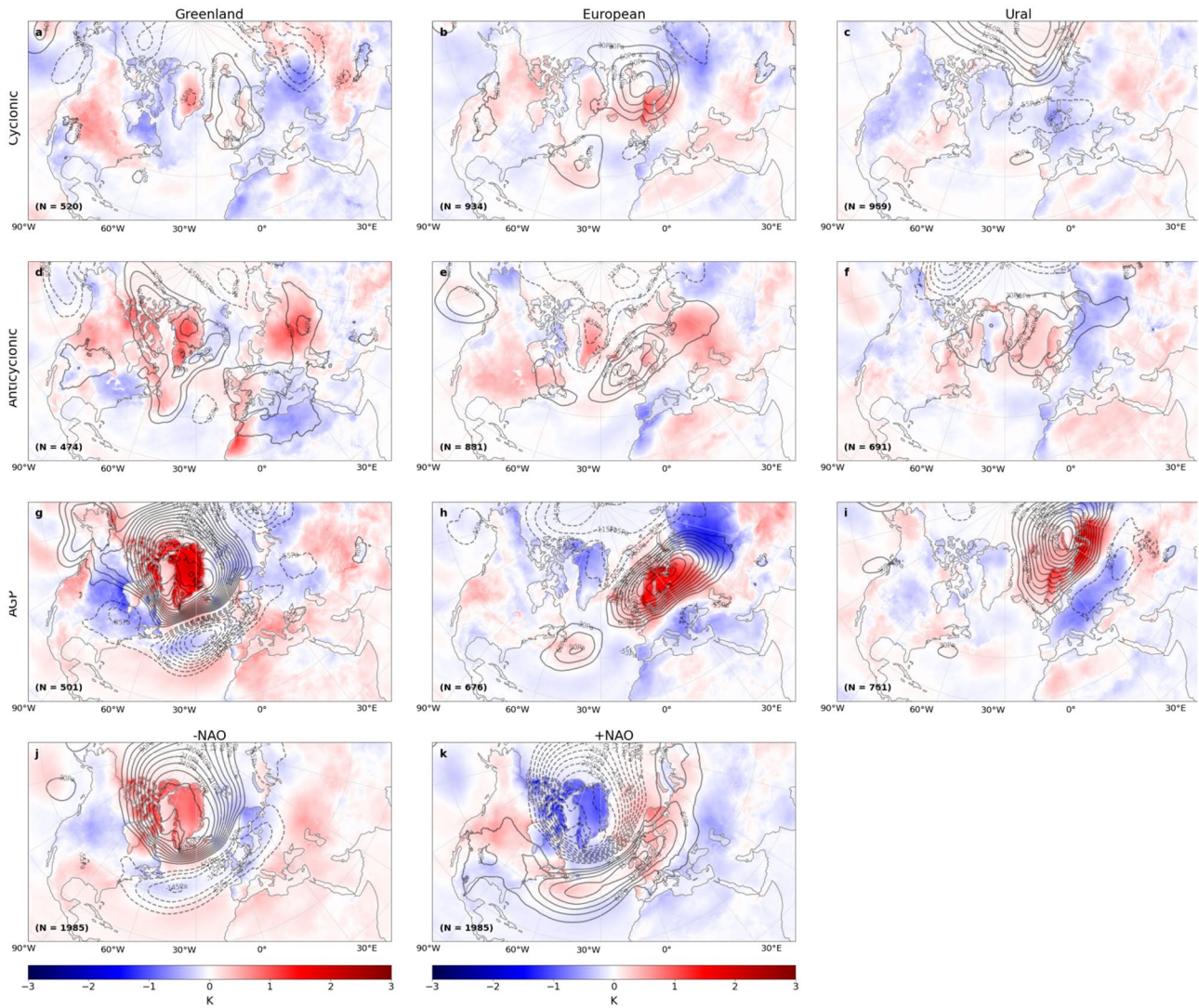


Fig. 14 The same as Figs. 10 and 12 but for JJA, showing daily blocking event and NAO composites by subregion and index for anomalous sea level pressure (contours) and two-meter temperature (blue-red shading). Contours are every 30 mb

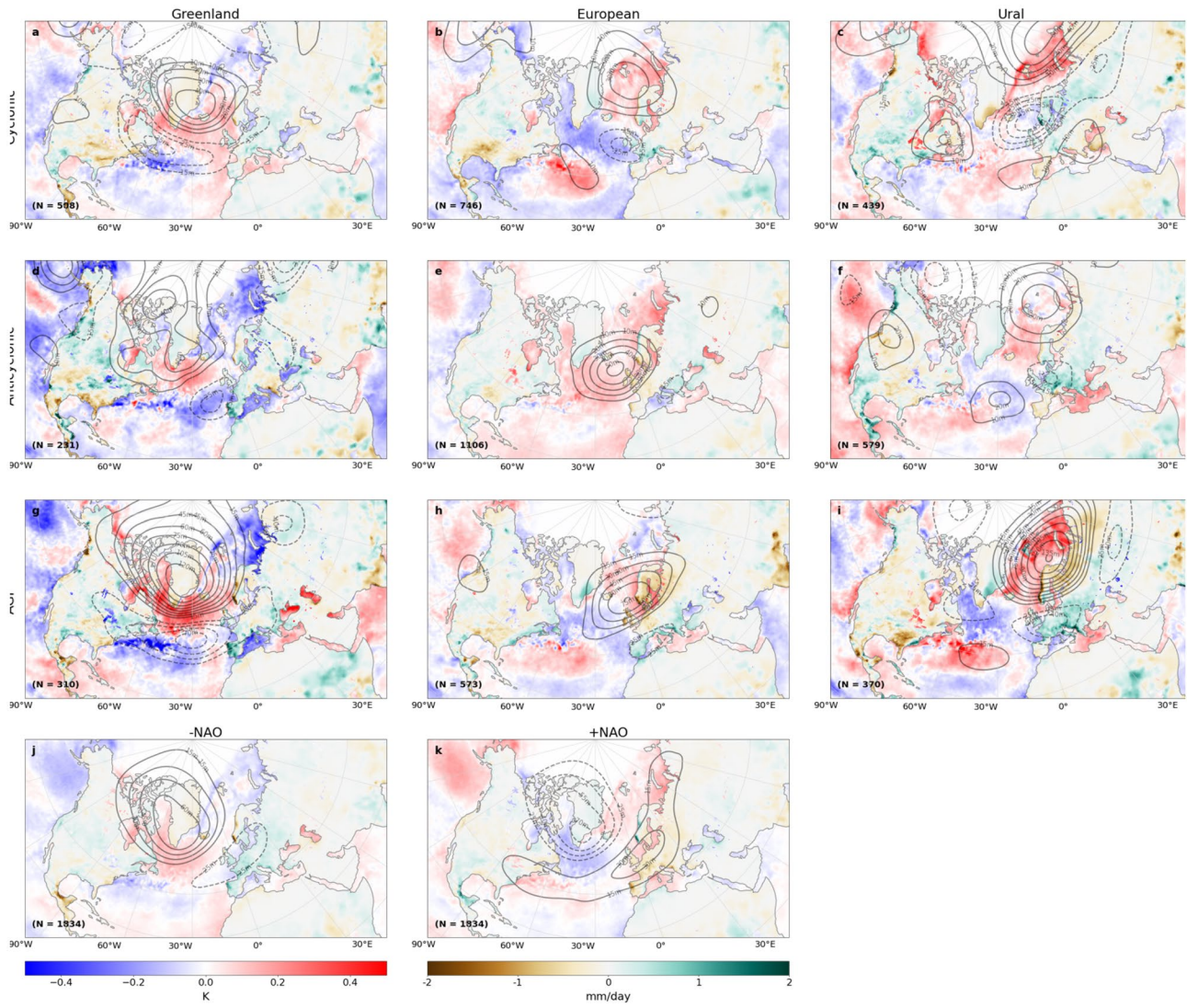


Fig. 15 The same as Figs. 9, 11, and 13 but for SON showing daily blocking event and NAO composites by subregion and index of anomalous Z500mb (black contours), precipitation (brown-green shading), and SSTs (blue-red shading)

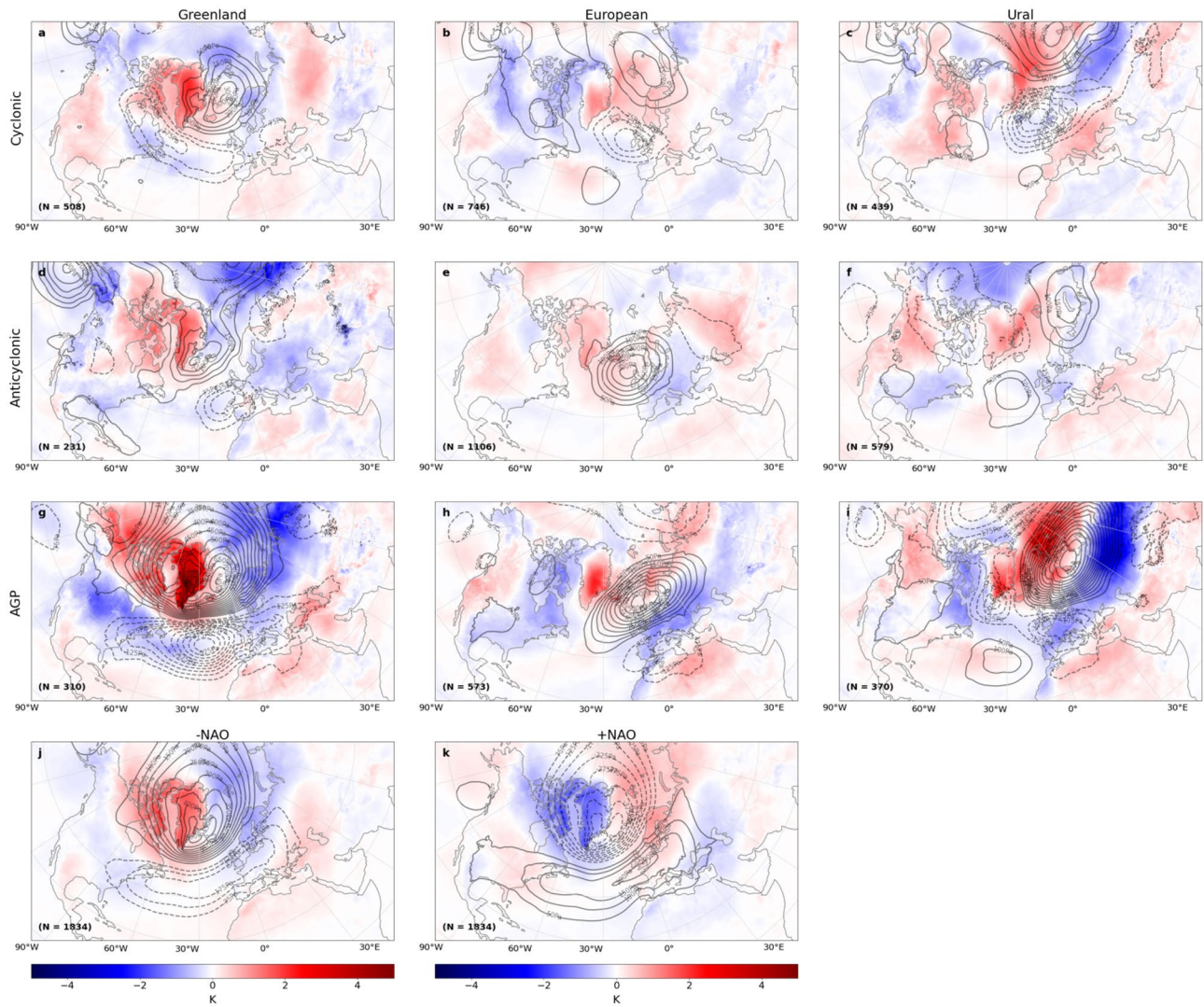


Fig. 16 The same as Figs. 10, 12, and 14 but for SON, showing daily blocking event and NAO composites by subregion and index for anomalous sea level pressure (contours) and two-meter temperature (blue-red shading). Contours are every 50 mb

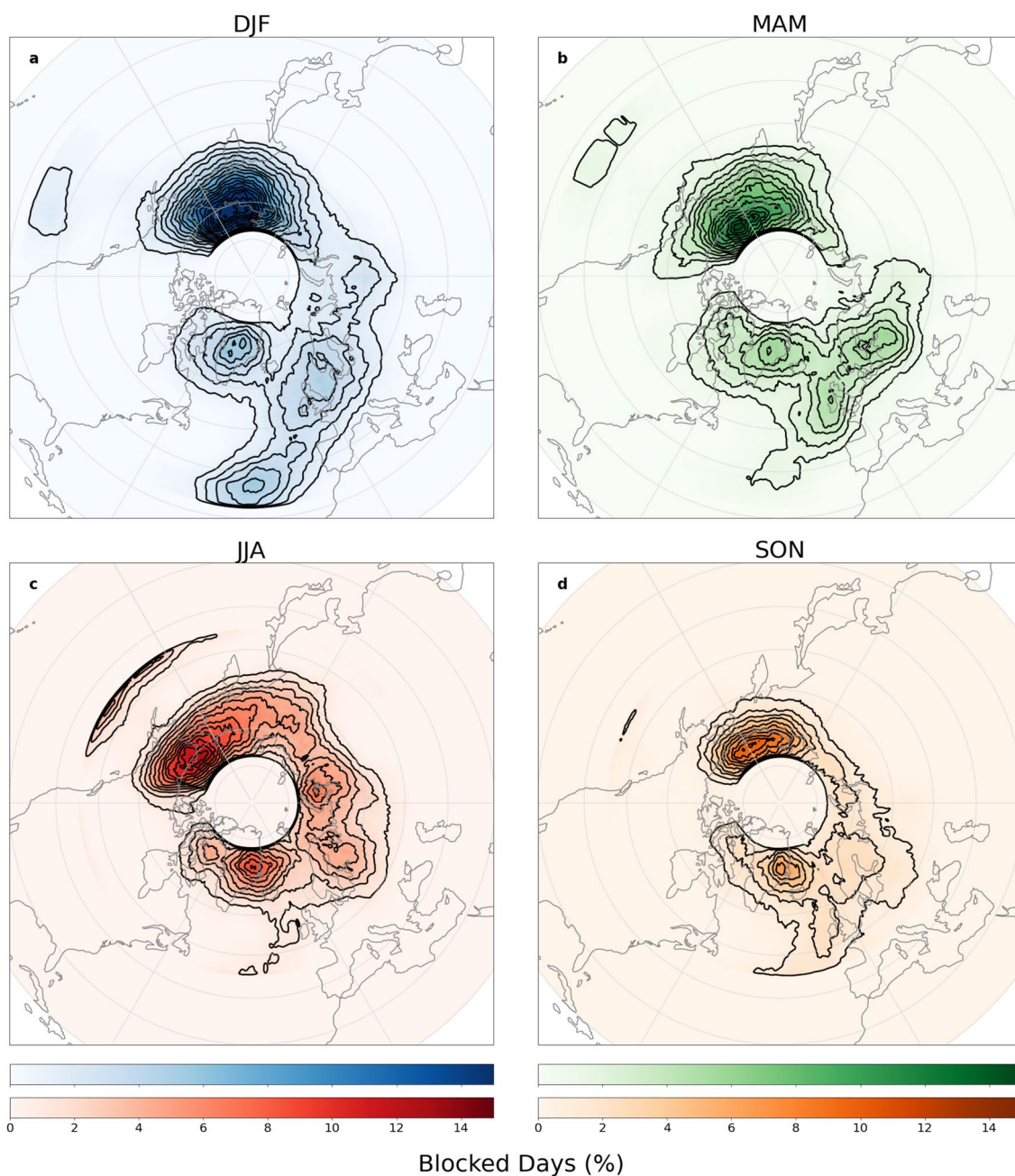


Fig. 17 Mean seasonal blocking frequency from 1980 to 2019 representing the average percent of blocked days per season when applying the absolute geopotential height (AGP) index. Contours are every 1%

Acknowledgements The authors would like to acknowledge the helpful insight gained from the reviewers.

Funding The authors acknowledge the support from National Oceanic and Atmospheric Administration (NA18OAR4310293, NA15OAR4320064, NA20OAR4320472), National Science Foundation (OCE1419569, OCE1559151), and Department of Energy (DE-SC0019433).

Data availability ERA5 reanalysis data used in this study can be found at <https://cds.climate.copernicus.eu/cdsapp#!/home>. The NAO index

used can be found at <https://psl.noaa.gov/data/gridded/data.cpc.globalprecip.html>. The datasets and algorithm generated during and/or analyzed during the current study are available from the corresponding author on reasonable request.

Declarations

Conflict of interest The authors have no relevant financial or non-financial interests to disclose.

Data citation Analysis was done in python heavily utilizing Xarray (Hoyer & Hamman 2017), matplotlib (Hunter 2007), scipy (Virtanen et al. 2020), pandas (McKinney 2010), jupyter lab (Jupyter et al. 2018), numpy (Harris et al. 2020), and dask (Dask 2016).

References

- Athanasiadis PJ, Yeager S, Kwon Y-O, Bellucci A, Smith DW, Tibaldi S (2020) Decadal predictability of North Atlantic blocking and the Nao. *Npj Clim Atmos Sci*. <https://doi.org/10.1038/s41612-020-0120-6>
- Benedict JJ, Lee S, Feldstein SB (2004) Synoptic view of the North Atlantic Oscillation. *AMETSOC*. https://journals.ametsoc.org/view/journals/atsc/61/2/1520-0469_2004_061_0121_svtovna_2.0.co_2.xml. Accessed 12 Jan 2023
- Benedict JJ, Clement AC, Medeiros B (2019) Atmospheric blocking and other large-scale precursor patterns of Landfalling Atmospheric Rivers in the North Pacific: a CESM2 study. *J Geophys Res Atmos* 124(21):11330–11353. <https://doi.org/10.1029/2019jd030790>
- Berrisford P, Hoskins BJ, Tyrlis E (2007) Blocking and rossby wave breaking on the dynamical tropopause in the Southern Hemisphere. *J Atmos Sci* 64(8):2881–2898. <https://doi.org/10.1175/jas3984.1>
- Bondur VG, Mokhov II, Voronova OS, Sitnov SA (2020) Satellite Monitoring of Siberian wildfires and their effects: features of 2019 anomalies and trends of 20-year changes. *Dokl Earth Sci* 492(1):370–375. <https://doi.org/10.1134/s1028334x20050049>
- Charney JG, DeVore JG (1979) Multiple flow equilibria in the atmosphere and blocking. *J Atmos Sci* 36(7):1205–1216. [https://doi.org/10.1175/1520-0469\(1979\)036%3c1205:mfeita%3e2.0.co;2](https://doi.org/10.1175/1520-0469(1979)036%3c1205:mfeita%3e2.0.co;2)
- Colucci SJ (1985) Explosive cyclogenesis and large-scale circulation changes: implications for atmospheric blocking. *J Atmos Sci* 42(24):2701–2717. [https://doi.org/10.1175/1520-0469\(1985\)042%3c2701:ecalse%3e2.0.co;2](https://doi.org/10.1175/1520-0469(1985)042%3c2701:ecalse%3e2.0.co;2)
- Colucci SJ (2001) Planetary-scale preconditioning for the onset of blocking. *J Atmos Sci* 58(8):933–942. [https://doi.org/10.1175/1520-0469\(2001\)058%3c0933:pspfto%3e2.0.co;2](https://doi.org/10.1175/1520-0469(2001)058%3c0933:pspfto%3e2.0.co;2)
- Croci-Maspoli M, Schwierz C, Davies HC (2007) Atmospheric blocking: space-time links to the NAO and pna. *Clim Dyn* 29(7–8):713–725. <https://doi.org/10.1007/s00382-007-0259-4>
- D’Andrea F, Tibaldi S, Blackburn M, Boer G, Déqué M, Dix MR, Dugas B, Ferranti L, Iwasaki T, Kitoh A, Pope V, Randall D, Roeckner E, Strauss D, Stern W, Van den Dool H, Williamson D (1998) Northern Hemisphere atmospheric blocking as simulated by 15 atmospheric general circulation models in the period 1979–1988. *Clim Dyn* 14(6):385–407. <https://doi.org/10.1007/s003820050230>
- Dask Development Team (2016). Dask: library for dynamic task scheduling. URL <https://dask.org>
- Davini P, Cagnazzo C (2013) On the misinterpretation of the North Atlantic oscillation in CMIP5 models. *Clim Dyn* 43(5–6):1497–1511. <https://doi.org/10.1007/s00382-013-1970-y>
- Davini P, D’Andrea F (2020) From CMIP3 to CMIP6: Northern Hemisphere atmospheric blocking simulation in present and future climate. *J Clim* 33(23):10021–10038. <https://doi.org/10.1175/jcli-d-19-0862.1>
- Davini P, Cagnazzo C, Gualdi S, Navarra A (2012) Bidimensional diagnostics, variability, and trends of Northern Hemisphere blocking. *J Clim* 25(19):6496–6509. <https://doi.org/10.1175/jcli-d-12-00032.1>
- Davini P, Corti S, D’Andrea F, Rivière G, von Hardenberg J (2017) Improved Winter European atmospheric blocking frequencies in high-resolution global climate simulations. *J Adv Model Earth Syst* 9(7):2615–2634. <https://doi.org/10.1002/2017ms001082>
- Demirtaş M (2018) The high-impact 2007 hot summer over Turkey: atmospheric-blocking and heat-wave episodes. *Meteorol Appl* 25(3):406–413. <https://doi.org/10.1002/met.1708>
- Elliott RD, Smith TB (1949) A study of the effects of large blocking highs on the general circulation in the northern-hemisphere westerlies. *J Meteorol* 6(2):68–85. [https://doi.org/10.1175/1520-0469\(1949\)006%3c0068:asoteo%3e2.0.co;2](https://doi.org/10.1175/1520-0469(1949)006%3c0068:asoteo%3e2.0.co;2)
- Fei H, Faxiu Z, Xiaodan Q (2002) Interannual and decadal variability of the North Pacific blocking and its relationship to SST, teleconnection and storm tracks. *Adv Atmos Sci* 19(5):807–820. <https://doi.org/10.1007/s00376-002-0046-4>
- Ferranti L, Magnusson L, Vitart F, Richardson DS (2018) How far in advance can we predict changes in large-scale flow leading to severe cold conditions over Europe? *Q J R Meteorol Soc* 144(715):1788–1802. <https://doi.org/10.1002/qj.3341>
- Haines K, Marshall J (1987) Eddy-forced coherent structures as a prototype of atmospheric blocking. *Q J R Meteorol Soc* 113(476):681–704. <https://doi.org/10.1002/qj.49711347613>
- Harris CR, Millman KJ, van der Walt SJ, Gommers R, Virtanen P, Cournapeau D, Wieser E, Taylor J, Berg S, Smith NJ, Kern R, Picus M, Hoyer S, van Kerkwijk MH, Brett M, Haldane A, del Río JF, Wiebe M, Peterson P, Oliphant TE (2020) Array programming with NumPy. *Nature* 585(7825):357–362. <https://doi.org/10.1038/s41586-020-2649-2>
- Hersbach H, Bell B, Berrisford P, Hirahara S, Horányi A, Muñoz-Sabater J, Nicolas J, Peubey C, Radu R, Schepers D, Simmons A, Soci C, Abdalla S, Abellan X, Balsamo G, Bechtold P, Biavati G, Bidlot J, Bonavita M, Thépaut JN (2020) The ERA5 global reanalysis. *Q J R Meteorol Soc* 146(730):1999–2049. <https://doi.org/10.1002/qj.3803>
- Hoskins BJ, Karoly DJ (1981) The steady linear response of a spherical atmosphere to thermal and orographic forcing. *J Atmos Sci* 38(6):1179–1196. [https://doi.org/10.1175/1520-0469\(1981\)038%3c1179:tslroa%3e2.0.co;2](https://doi.org/10.1175/1520-0469(1981)038%3c1179:tslroa%3e2.0.co;2)
- Hoyer S, Hamman JJ (2017) Xarray: N-D labeled arrays and datasets in Python. *J Open Res Softw*. <https://doi.org/10.5334/jors.148>
- Hunter JD (2007) Matplotlib: a 2D graphics environment. *Comput Sci Eng* 9(3):90–95. <https://doi.org/10.1109/mcse.2007.55>
- Jung T, Hilmer M, Ruprecht E, Kleppek S, Gulev SK, Zolina O (2003) Characteristics of the recent eastward shift of interannual Nao variability. *J Clim* 16(20):3371–3382. [https://doi.org/10.1175/1520-0442\(2003\)016%3c3371:cotres%3e2.0.co;2](https://doi.org/10.1175/1520-0442(2003)016%3c3371:cotres%3e2.0.co;2)
- Jung T, Miller MJ, Palmer TN, Towers P, Wedi N, Achuthavariar D, Adams JM, Altshuler EL, Cash BA, Kinter JL, Marx L, Stan C, Hodges KI (2012) High-resolution global climate simulations with the ECMWF model in Project Athena: experimental design, model climate, and seasonal forecast skill. *J Clim* 25(9):3155–3172. <https://doi.org/10.1175/jcli-d-11-00265.1>
- Jupyter P, Bussonnier M, Forde J, Freeman J, Granger B, Head T, Holdgraf C, Kelley K, Nalvarte G, Osheroff A, Pacer M, Panda Y, Perez F, Ragan-Kelley B, Willing C (2018) Binder 2.0—reproducible, interactive, sharable environments for science at scale. In: Proceedings of the python in science conference. <https://doi.org/10.25080/majora-4af1f417-011>
- Legras B, Ghil M (1985) Persistent anomalies, blocking and variations in atmospheric predictability. *J Atmos Sci* 42(5):433–471. [https://doi.org/10.1175/1520-0469\(1985\)042%3c0433:pabavi%3e2.0.co;2](https://doi.org/10.1175/1520-0469(1985)042%3c0433:pabavi%3e2.0.co;2)
- Lejenäs H, Madden RA (1992) Traveling planetary-scale waves and blocking. *Mon Weather Rev* 120(12):2821–2830. [https://doi.org/10.1175/1520-0493\(1992\)120%3c2821:tpswab%3e2.0.co;2](https://doi.org/10.1175/1520-0493(1992)120%3c2821:tpswab%3e2.0.co;2)

- Lucarini V, Gritsun A (2019) A new mathematical framework for atmospheric blocking events. *Clim Dyn* 54(1–2):575–598. <https://doi.org/10.1007/s00382-019-05018-2>
- Luo D, Gong T (2006) A possible mechanism for the eastward shift of Interannual Nao Action Centers in last three decades. *Geophys Res Lett*. <https://doi.org/10.1029/2006gl027860>
- Ma J, San Liang X (2017) Multiscale dynamical processes underlying the wintertime Atlantic blockings. *J Atmos Sci* 74(11):3815–3831. <https://doi.org/10.1175/jas-d-16-0295.1>
- Masato G, Hoskins BJ, Woollings TJ (2009) Can the frequency of blocking be described by a red noise process? *J Atmos Sci* 66(7):2143–2149. <https://doi.org/10.1175/2008jas2907.1>
- Masato G, Hoskins BJ, Woollings TJ (2011) Wave-breaking characteristics of Midlatitude blocking. *Q J R Meteorol Soc* 138(666):1285–1296. <https://doi.org/10.1002/qj.990>
- Masato G, Hoskins BJ, Woollings T (2013) Wave-breaking characteristics of northern hemisphere winter blocking: a two-dimensional approach. *J Clim* 26:4535–4549. <https://doi.org/10.1175/JCLI-D-12-00240.1>
- McKinney W (2010) Data structures for statistical computing in python. In: *Proceedings of the Python in science conference*. <https://doi.org/10.25080/majora-92bf1922-00a>
- McWilliams JC (1980) An application of equivalent modons to atmospheric blocking. *Dyn Atmos Oceans* 5(1):43–66. [https://doi.org/10.1016/0377-0265\(80\)90010-x](https://doi.org/10.1016/0377-0265(80)90010-x)
- Nakamura H (1994) Rotational evolution of potential vorticity associated with a strong blocking flow configuration over Europe. *Geophys Res Lett* 21(18):2003–2006. <https://doi.org/10.1029/94gl01614>
- Pelly JL, Hoskins BJ (2003) A new perspective on blocking. *J Atmos Sci* 60(5):743–755. [https://doi.org/10.1175/1520-0469\(2003\)060%3c0743:anpob%3e2.0.co;2](https://doi.org/10.1175/1520-0469(2003)060%3c0743:anpob%3e2.0.co;2)
- Pfahl S, Wernli H (2012) Quantifying the relevance of atmospheric blocking for co-located temperature extremes in the Northern Hemisphere on (sub-)daily Time Scales. *Geophys Res Lett*. <https://doi.org/10.1029/2012gl052261>
- Pinheiro MC, Ullrich PA, Grotjahn R (2019) Atmospheric blocking and Intercomparison of objective detection methods: flow field characteristics. *Clim Dyn* 53(7–8):4189–4216. <https://doi.org/10.1007/s00382-019-04782-5>
- Rex DF (1950) Blocking action in the middle troposphere and its effect upon regional climate. *Tellus* 2(3):196–211. <https://doi.org/10.1111/j.2153-3490.1950.tb00331.x>
- Scaife AA, Woollings T, Knight J, Martin G, Hinton T (2010) Atmospheric blocking and mean biases in climate models. *J Clim* 23(23):6143–6152. <https://doi.org/10.1175/2010jcli3728.1>
- Scaife AA, Copesey D, Gordon C, Harris C, Hinton T, Keeley S, O'Neill A, Roberts M, Williams K (2011) Improved Atlantic winter blocking in a climate model. *Geophys Res Lett*. <https://doi.org/10.1029/2011gl049573>
- Scherrer SC, Croci-Maspoli M, Schwierz C, Appenzeller C (2006) Two-dimensional indices of atmospheric blocking and their statistical relationship with winter climate patterns in the Euro-Atlantic Region. *Int J Climatol* 26(2):233–249. <https://doi.org/10.1002/joc.1250>
- Shabbar A, Huang J, Higuchi K (2001) The relationship between the wintertime North Atlantic Oscillation and blocking episodes in the North Atlantic. *Int J Climatol* 21(3):355–369. <https://doi.org/10.1002/joc.612>
- Sousa PM, Barriopedro D, García-Herrera R, Woollings T, Trigo RM (2021) A new combined detection algorithm for blocking and subtropical ridges. *J Clim*. <https://doi.org/10.1175/jcli-d-20-0658.1>
- Takaya K, Nakamura H (2005) Geographical dependence of upper-level blocking formation associated with intraseasonal amplification of the Siberian high. *J Atmos Sci* 62(12):4441–4449. <https://doi.org/10.1175/jas3628.1>
- Tibaldi S, Tosi E, Navarra A, Pedulli L (1994) Northern and southern hemisphere seasonal variability of blocking frequency and predictability. *Mon Weather Rev* 122(9):1971–2003. [https://doi.org/10.1175/1520-0493\(1994\)122%3c1971:nashsv%3e2.0.co;2](https://doi.org/10.1175/1520-0493(1994)122%3c1971:nashsv%3e2.0.co;2)
- Trigo RM, Trigo IF, DaCamara CC, Osborn TJ (2004) Climate impact of the European winter blocking episodes from the NCEP/NCAR reanalyses. *Clim Dyn* 23(1):17–28. <https://doi.org/10.1007/s00382-004-0410-4>
- Tyrlis E, Hoskins BJ (2008a) Aspects of a Northern Hemisphere atmospheric blocking climatology. *J Atmos Sci* 65(5):1638–1652. <https://doi.org/10.1175/2007jas2337.1>
- Tyrlis E, Hoskins BJ (2008b) The morphology of Northern Hemisphere blocking. *J Atmos Sci* 65(5):1653–1665. <https://doi.org/10.1175/2007jas2338.1>
- Ulbrich U, Christoph M (1999) A shift of the NAO and increasing storm track activity over Europe due to anthropogenic greenhouse gas forcing. *Clim Dyn* 15(7):551–559. <https://doi.org/10.1007/s003820050299>
- Virtanen P, Gommers R, Oliphant TE, Haberland M, Reddy T, Cournapeau D, Burovski E, Peterson P, Weckesser W, Bright J, van der Walt SJ, Brett M, Wilson J, Millman KJ, Mayorov N, Nelson AR, Jones E, Kern R, Larson E, Vázquez-Baeza Y (2020) SciPy 1.0: Fundamental algorithms for scientific computing in python. *Nat Methods* 17(3):261–272. <https://doi.org/10.1038/s41592-019-0686-2>
- Wise EK (2016) Five centuries of U.S. west coast drought: occurrence, spatial distribution, and associated atmospheric circulation patterns. *Geophys Res Lett* 43(9):4539–4546. <https://doi.org/10.1002/2016gl068487>
- Woollings T, Hoskins B, Blackburn M, Berrisford P (2008) A new Rossby wave–breaking interpretation of the North Atlantic Oscillation. *J Atmos Sci* 65(2):609–626. [https://doi.org/10.1175/2007j as2347.1](https://doi.org/10.1175/2007jas2347.1)
- Woollings T, Barriopedro D, Methven J, Son S-W, Martius O, Harvey B, Sillmann J, Lupo AR, Seneviratne S (2018) Blocking and its response to climate change. *Curr Clim Change Rep* 4(3):287–300. <https://doi.org/10.1007/s40641-018-0108-z>
- Yao Y, Luo D (2018) An asymmetric spatiotemporal connection between the Euro-Atlantic blocking within the NAO Life Cycle and European climates. *Adv Atmos Sci* 35(7):796–812. <https://doi.org/10.1007/s00376-017-7128-9>

Publisher's Note Springer Nature remains neutral with regard to jurisdictional claims in published maps and institutional affiliations.

Springer Nature or its licensor (e.g. a society or other partner) holds exclusive rights to this article under a publishing agreement with the author(s) or other rightsholder(s); author self-archiving of the accepted manuscript version of this article is solely governed by the terms of such publishing agreement and applicable law.